Published in final edited form as:
Liq Cryst Rev. 2013 ; 1(1): 29–51. doi:10.1080/21680396.2013.769310.

Chemical and biological sensing using liquid crystals

Rebecca J. Carlton, **Jacob T. Hunter**, **Daniel S. Miller**, **Reza Abbasi**, **Peter C. Mushenheim**, **Lie Na Tan**, and **Nicholas L. Abbott**
Department of Chemical and Biological Engineering, University of Wisconsin-Madison, Madison, Wisconsin 53706

Abstract

The liquid crystalline state of matter arises from orientation-dependent, non-covalent interaction between molecules within condensed phases. Because the balance of intermolecular forces that underlies formation of liquid crystals is delicate, this state of matter can, in general, be easily perturbed by external stimuli (such as an electric field in a display). In this review, we present an overview of recent efforts that have focused on exploiting the responsiveness of liquid crystals as the basis of chemical and biological sensors. In this application of liquid crystals, the challenge is to design liquid crystalline systems that undergo changes in organization when perturbed by targeted chemical and biological species of interest. The approaches described below revolve around the design of interfaces that selectively bind targeted species, thus leading to surface-driven changes in the organization of the liquid crystals. Because liquid crystals possess anisotropic optical and dielectric properties, a range of different methods can be used to read out the changes in organization of liquid crystals that are caused by targeted chemical and biological species. This review focuses on principles for liquid crystal-based sensors that provide an optical output.

Keywords

Liquid crystals; anchoring transitions; surfaces; biomolecular interfaces; chemically functionalized interfaces; biological sensors; chemical sensors; toxic chemicals; nerve agents; proteins; lipids; DNA; viruses; bacteria; cells

Introduction

Liquid crystals (LCs) have a long history of being used as responsive materials in a range of technologies, perhaps most obviously in the now-ubiquitous LC display. In an LC display, an electric field of predetermined strength is applied to the LC to drive it through a change in orientation and thus optical appearance. Although LC display technology is based on fundamental studies performed in 1927, it is only in the past 20 years that it has been widely adopted. In those studies, it was discovered that the orientations of rod-shaped LCs (and intensity of light transmitted through them) could be changed by application of an electric field across the LC [1, 2]. This phenomenon can be viewed as an example of the use of a LC

abbott@engr.wisc.edu.

as an actuator (light-shutter) [3-7]. Elastomeric materials made with LC components have also been used as mechanical actuators that undergo a change in shape in response to a predefined stimulus (e.g. change of temperature) [8]. Conversely, LCs can be used as sensors. In this context, the responsive nature of the LC remains important, but the response of the LC is used to indicate the appearance of a stimulus. Past studies have demonstrated that LC-based sensors can be designed to report a range of physical stimuli, including mechanical shear, temperature, electric and magnetic fields, and light. For example, Marcos et al. [9] reported the use of LCs to sense shear and temperature fields, Herzer et al. [10] reported printable cholesteric LC films as temperature and humidity sensors, and Chatterjee et al. [11] examined the influence of shear fields on defects in LCs. In addition, Chanishvili et al. [12] reported cholesteric LC mixtures that are sensitive to different ranges of solar UV radiation. Nematic LCs can also be doped with light-driven chiral switches that can be used to tune the pitch of the chiral phase [13].

While the paragraph above indicates that the responsive nature of LCs has been leveraged in the past to create actuators and sensors of a range of physical phenomena, this review moves to address a more recent effort that has been focused on the design of LCs as materials that respond to targeted chemical and biological species. As described in the various sections of this review, a series of recent publications have demonstrated the use of LCs to amplify molecular events into macroscopic signals, and thus potentially provide the basis of new classes of cheap, rapid, and label-free sensors. This review is focused on the use of LC-based *interfaces* for the creation of chemical and biological sensors, but, prior to detailing those studies, we note that several research groups have also reported the design of LC-based sensors for chemical and biological species based on changes in the *bulk* properties of LCs. For example, cholesteric LC phases have been used to detect ethanol [14], water vapour (via hydrolysis of a cholesteric dopant) [15], and vaporous analytes [16-18] such as amines [19, 20]. Those papers lie outside the scope of this review, and the interested reader is referred to the above-listed references for additional details.

In closing this introduction, we comment that the use of LCs for chemical and biological sensing defines a range of fundamental and technical challenges. For example, relative to LC display technologies, the interfacial phenomena encountered in the design of LC-based sensors are far more varied, complex, and challenging. The diversity of chemical functional groups that are presented by targeted chemical and biological analytes is far greater than the relatively simple polymeric surfaces that are typically used in LC display technologies (compare the complexity of a protein to a polyimide). This makes *a priori* prediction of the orientations that LCs assume on surfaces decorated with targeted analytes a particular (and largely unresolved) challenge. In addition, charges (e.g. ionic species) are ubiquitous in gas and liquid phases of relevance to sensing (e.g. a sample of water), and thus the interfaces of LCs charge as a consequence of ion adsorption/dissociation leading, for example, to the formation of electrical double layers at the interface of the LC which influence the ordering of the LC [21, 22]. Finally, because LC sensors must be open systems in order to interact with analytes, design of mechanically stable, open, microsystems containing LCs requires additional investigation and optimization. For example, mechanical stabilization of micrometer-thick films of LC remains a challenge under the conditions relevant to many

practical sensing environments, although recent advances on this front appear promising [23].

The remainder of this review is organized into five sections. The first section describes the detection of gas-phase analytes using a thin-film LC sensor. Second, we examine the use of LCs for the imaging of biomolecules displayed at solid surfaces. Next, we move to a discussion of biomolecular sensing at the dynamic LC-aqueous interface. Fourth, we address the use of LC emulsion droplets as a sensing platform. The last section (section 5) of this review focuses on progress related to the use of LCs as sensors of viruses, bacteria and mammalian cells. In each of the above-described sections, we highlight unresolved fundamental and technical challenges, and suggest areas for future research.

1. Gas sensing based on LCs

The first topic that we address in this review involves the use of LCs to create sensors for targeted chemical species present in a gas phase. Examples of important gas phase analytes include: (i) organophosphonates (OP) that are the basis of many nerve agents and pesticides; (ii) chlorine and ammonia, which are representative of a wide range of toxic industrial chemicals (TICs); (iii) chemicals found in exhaled breath that are associated with the health of a patient, including nitric oxide for asthma and ketones for diabetes; (iv) organoamines that indicate the freshness of foods; and (v) hazardous gases found in workplaces such as aldehydes and volatile organic compounds (VOCs). Because of the broad importance of detection of these and other gases, a large investment has been made in development of gas sensing technologies such as ion-mobility spectrometry (IMS), surface acoustic wave (SAW) devices, quartz crystal microbalances (QCM), and metal oxide-based sensors. Each existing technology, however, has attributes that limit its utility. A common disadvantage of these techniques, for example, is that they are limited in the range of species that can be detected. This is true, in particular, for IMS, where the length of the drift-tube must be matched to the targeted analytes. A second common challenge is instrumental sensitivity. A sensor for sarin needs, for example, to detect the nerve agent with a concentration that is under the CDC airborne exposure limit, which is approximately 20 ppb [24]. This concentration range is a challenge for many sensing technologies, and significantly, for other gases considered occupational hazards in the workplace (e.g. NO_2 from vehicle exhaust), evolving regulatory requirements are placing exposure limits at even lower concentrations. Finally, we comment that water (i.e. relative humidity) is a common interfering agent in gas sensing technologies. Dealing with variations in humidity and the chemical complexity of industrial workplaces and homes (e.g. a kitchen) remains a central challenge for many sensing technologies [25]. In the sections below, we describe efforts to develop LC-based gas sensing approaches that have been motivated, in large part, by the goal of addressing some of the above-listed limitations of existing gas sensing technologies.

A schematic illustration of the principle of operation of a surface-based LC sensor for gas-phase chemicals is shown in Figure 1 [26]. The sensor comprises a micrometer-thick film of LC that is supported on a chemically functionalized solid surface and exposed to a gas (e.g. air) that contains the vapour-phase analyte to be detected. The analyte diffuses across the LC film and binds to the chemically functionalized solid surface, leading to a change in the

alignment of the LC at the solid surface, as shown in Figure 1A. A key element of the gas sensor is the design of the interface between the LC and the solid. In the examples shown in Figure 1, the chemically functionalized solid surface is selected to align the LC in a preferred azimuthal (Figure 1B) or zenithal alignment (Figure 1D) in the absence of the analyte. Upon binding of the analyte to the chemically functionalized surface, the molecular interactions between the solid surface and the LC are perturbed. This exchange of molecular interactions (i.e. competitive binding of the LC and targeted analyte for the surface) leads to a change in the azimuthal (Figure 1C) or zenithal alignment (Figure 1E) of the LC, thus reporting the presence of the vapour analyte [26].

As noted above, the design principles underlying LC gas sensors are based on the engineering of competitive interactions between the chemical functional groups of the mesogens and the vapour analyte for the solid surface. Manipulation of the chemically functionalized solid surface can, therefore, be used to change the selectivity of the LC-based sensor (i.e. which compound is detected by the sensor) [26-29]. To date, this approach has been exploited to develop LC-based sensors that can detect organophosphonate compounds [26, 30], organoamines [31], aldehydes [32] and organosulfur [33] compounds. Below we focus on two of these examples to illustrate attributes of LC-based gas sensors.

The first example that we describe below addresses detection of organophosphonates using surfaces decorated with perchlorate salts. The design of the sensor is based on the observation that LCs comprised of mesogens with nitrile groups (e.g. 5CB, 8CB, or E7) will assume a homeotropic (perpendicular) alignment on surfaces decorated with metal perchlorate salts with cations that have a high electron affinity. For example, and as illustrated in Figure 2A-C, copper (II) perchlorate forms a coordination complex with nitrile-containing mesogens (e.g. 5CB), causing a homeotropic alignment of nematic phases of 5CB. Because the LC also assumes a homeotropic alignment in contact with air, such an LC film exhibits a dark appearance when viewed between crossed polarisers [26]. Evidence for formation of a coordination complex between the nitrile groups of LCs and the Cu (II) ions on the surface has been obtained using infrared spectroscopy (Figure 2D). Inspection of Figure 2D-i reveals a nitrile-stretch absorption peak at 2227 cm^{-1}, which corresponds to free nitrile groups, and a second peak at 2287 cm^{-1} that corresponds to the nitrile groups of 8CB in coordination with Cu (II). As reported elsewhere [27, 34], by changing the metal cation in the perchlorate salt, it has been demonstrated that the presence of a coordination interaction between the nitrile group and the metal cation is correlated to the observation of homeotropic alignment of the LC. This observation supports the hypothesis that the orientation of the LCs can be predictably manipulated based on metal-ligand coordination interactions at surfaces.

As described above, the initial orientation of an LC in a sensor based on the use of metal salts is determined by metal ion-ligand coordination interactions between the LC and metal salt on the surface. When using Cu (II) as the metal ion in the salt, the introduction of dimethyl methylphosphonate (DMMP) into the system has been shown to result in the preferential binding of DMMP to the Cu (II) ions over the nitrile groups of the LC. This change in interfacial interaction is evidenced by a change in the alignment of the LC from homeotropic to planar, with an associated increase in the amount of light transmitted

through the LC film when viewed between crossed polarisers (Figure 2A-C) [26]. The molecular basis of the change in orientation of the LC has also been supported by infrared measurements. Upon exposure to a vapour phase containing 10 ppm DMMP, as shown in Figure 2D-ii, the absorption peak corresponding to the metal ion-coordinated state of the nitrile group of 8CB (at 2287 cm^{-1}) was observed to disappear [34]. The response of the LC to DMMP was found to be reversible, meaning that the orientation of the LC returns to the homeotropic state after the DMMP is removed from the vapour space above the LC film (see Figure 2E). Furthermore, the return of the LC to the homeotropic state was accompanied by the reappearance of the peak corresponding to the coordinated nitrile group in the infrared spectrum (Figure 2D-iii) [26]. Here we also note that exposure of the LC sensors to vapours of water, alkanes and various other organic compounds (alcohols, ketones etc) does not lead to a response (i.e. change in orientation of the LC) because these compounds cannot displace the nitrile groups of the LC from coordination with the Cu (II) at the surface.

The molecular engineering principles described above – an LC sensor based on competitive coordination interactions at metal ion-decorated surfaces – is a general one, as a range of different metal ions (or more broadly, chemical functional groups) can be presented at the surfaces of solids to manipulate the selectivity of the sensor. As an example, Figure 3 shows results obtained with surfaces that presented aluminium (III), zinc (II), or iron (III) perchlorate salts. Whereas LCs supported on surfaces presenting Al (III) salts responded to all four organophosphonate nerve agents (GB, GD, GA and VX), the surfaces with Zn (II) reported only GB and VX, and the surfaces with Fe (III) reported GB but not VX [30]. An additional design parameter that can be used to tune the response of an LC sensor is the chemical structure of the mesogens used to form the LC phase. For example, mesogens that possess two nitrile groups have been synthesized, and LC phases containing these tailored mesogens exhibited homeotropic alignments on metal ion-decorated surfaces under conditions that LCs containing a single nitrile group do not. Specifically, we have measured bivalent mesogens to align on surfaces presenting very low concentrations of Al (III) ions on surfaces [35].

While the studies described above highlight the role that coordination interactions can play in the design of gas sensors based on LCs, we also note that surfaces decorated with metal salts are complex and remain to be fully understood. For example, it has recently been established that metal salts on surfaces can dissolve partially into the LC, leading to the formation of electrical double layers. The presence of the electrical double layers can influence the alignment of the LC and thus the response of the sensors to targeted compounds [21, 36]. Additional aspects of the interfacial designs of these sensors that remain to be fully understood include the role of the counter-ions (the above described results were based on perchlorate salts) and the properties of the surface that support the metal salts [29, 37].

The second example of chemical sensing using LCs that we describe in this review involves detection of organoamines. In this example, the sensors are based on surfaces that possess anisotropic topography and present carboxylic acid groups. The design of the sensor exploits competitive topographic and molecular-level interactions to drive anchoring transitions upon

exposure to targeted analytes. The topographic interactions were engineered into the surfaces via an anisotropic topography consisting of grooves with an amplitude of 1-2 nm and a wavelength of 10-30 nm. The topography causes the LC to align in an azimuthal orientation that is parallel to the grooves (Figure 1C). However, when the surfaces were decorated with an organized monolayer presenting oriented carboxylic acids groups, hydrogen bonding of the mesogens to the acid groups displayed by the surface caused the LC to assume an orientation that was perpendicular to the grooves (Figure 1B) [38]. The role of hydrogen bonding in determining the orientations of LCs on these surfaces is supported by the results of infrared spectroscopy. Figure 4A-i shows the infrared spectrum of a carboxylic acid-terminated monolayer. The absorbance peaks indicate the presence of a mixture of non-hydrogen-bonded carbonyl groups (peak at 1736 cm^{-1}) and hydrogen-bonded carbonyl groups (peak at 1716 cm^{-1}). A schematic illustration of such a surface is shown in Figure 4B-i. When the surface is contacted with 8CB, as shown in Figure 4A-ii, a decrease is observed in the absorption peak in the infrared spectrum corresponding to intra-monolayer hydrogen bonding, consistent with competitive formation of hydrogen bonds between the nitrile group of the mesogen and the carboxylic acid groups on the surface (Figure 4B-ii) [38].

Upon introduction of an amine compound, an acid-base reaction occurs between the carboxylic acid and the amine (resulting in the formation of an ammonium carboxylate salt), thus disrupting the hydrogen bonding between the LC and the surface, as described above. In the absence of the hydrogen-bonding interaction, the LC relaxes to an orientation on the surface that is dictated by the topography of the surface. The change in the azimuthal alignment of the LC can be optically detected through crossed polarisers, as shown in Figure 4C. Here we end our discussion of this LC sensor design by noting that it is possible to design systems that quantify the diffusion of an analyte *laterally* through a thin film of LC confined between two solid surfaces. Figure 4D shows the distance that hexylamine has diffused laterally across a film of LC, revealing that the penetration distance of the analyte is proportional to the square root of the exposure time (consistent with passive transport of the amine via diffusion) [31]. This geometry of the LC sensor is a promising one for quantification of the cumulative exposure of the sensor to a targeted analyte (e.g. for measurement of personal exposure to potentially hazardous chemical environments).

2. LC-based sensing of biomolecules displayed on surfaces

The second class of LC-based sensors that we address in this review is aimed at reporting the presence of biological molecules, such as proteins, oligopeptides, and nucleic acids, displayed on the surfaces of solids. Inspired by the remarkable sensitivity of the ordering of LCs to the chemical functionality and organization of molecules at interfaces, LC sensors have been used to report a range of biomolecules and their orientations on solid surfaces [39-42]. While technologies for reporting biomolecules at surfaces (in contexts such as environmental monitoring, medical diagnostics, food safety and biosecurity) have been developed, existing approaches typically involve the use of complex instrumentation (e.g. mass spectroscopy and evanescent optical methods such as surface plasmon resonance) or schemes that involve the labelling of molecules with fluorescent, redox-active, or radio-active tags.

In the approaches described below for LC-based detection of biomolecules, the surfaces of solids are designed with carefully selected chemical functionality and nanoscopic topography. Following capture of the targeted biomolecular species on the solid surface (typically via a specific binding event), the surface is contacted with LC. The surface is designed such that the captured biomolecules change either the energy of interaction of the LC with the surface (anchoring energy, W) or the preferred orientation of the LC (easy axis). In this section, we will highlight several studies that illustrate the potential utility of LCs for imaging surfaces decorated by proteins, oligopeptides, or DNA.

2.1 Proteins

The first examples that we address involve the detection of proteins. Past studies have demonstrated that LCs can be used to image proteins captured on solid surfaces via specific protein-small molecule or protein-protein interactions. In addition, as described below, LCs can also be used to image proteins that have been printed (non-specifically adsorbed) onto a surface in the context of analytic schemes based on affinity contact printing (with a spatial resolution of tens of micrometers). These results suggest that LCs may offer the basis of label-free and highly multiplexed methods for protein analysis [39, 43-45].

The first report of the use of chemically functionalized surfaces for LC-based protein detection was published by Gupta et al. [40]. Specifically, this report demonstrated that nematic LCs can be used to amplify and transduce receptor-mediated binding of proteins at surfaces into readily observable optical responses. Organized monolayers (so-called self-assembled monolayers or SAMs) of ligands capable of binding targeted proteins were formed on the surfaces of obliquely deposited gold films. Ordinarily, such obliquely deposited gold films impart a uniform azimuthal alignment to LCs. When either avidin or anti-biotin antibodies (IgG) were incubated against SAMs presenting the binding group called biotin, the anisotropic topography of the obliquely deposited gold films was masked by the bound protein layer such that the LCs exhibited non-uniform orientations on the surfaces. In addition, the authors demonstrated that it was possible to tune the surface topography of the gold films (by changing the angle of deposition of the gold during physical vapour deposition) such that the capture of an antibody by a surface immobilized protein resulted in a measurable change in the alignment of the LC [40].

Building from the results of the above study, Skaife and Abbott [44] demonstrated that it was possible to quantify the optical response of LCs, and thus the amount of protein captured at a surface, by measuring the fraction of polarized light transmitted through the LC. The optical response (quantified as a gray-scale brightness) was observed to be a continuous function of the amount of bound protein. Because the amount of bound IgG was largely determined by mass transfer of antibody to the surface, quantification of the LC optical response allowed for determination of the bulk IgG concentration over two orders of magnitude (1-100nM) [44].

In contrast to many other methods used for imaging biomolecules at surfaces, a distinguishing feature of LC-based methods is that the LCs can probe the structure of the biomolecules displayed at the surface. This attribute is illustrated in a study by Luk et al. [46] that investigated the binding of ribonuclease A (RNase A) with the ribonuclease

inhibitor protein (RI). Although ellipsometry reported the effective optical thickness of RNase A to be identical in two methods of surface preparation, the orientation assumed by the 5CB on the surface with RNase A immobilized in random orientations was different from the orientation observed for 5CB on the surface with RNase A immobilized in a preferred orientation. This result indicates that the orientational states of proteins immobilized on surfaces can be distinguished by examining the optical response of the LC [46].

An additional useful attribute of LC-based imaging of biomolecules on surfaces is that LCs can be used to detect proteins captured on surfaces via a wide range of binding groups. For example, Clare and Abbott [47] investigated the orientations of 5CB in contact with surfaces that presented oligopeptides for specific binding of proteins. In particular, surfaces functionalized with the oligopeptide-substrate for the Src protein kinase (Src-tide) and its phosphorylated synthetic equivalent (p-Src-tide) were studied (Figure 5A, see Figure 5B for protein structures). The time required for a contacting film of 5CB to adopt a uniform homeotropic orientation on the surface was demonstrated to increase with increasing areal densities of immobilized peptides. Furthermore, it was demonstrated that specific binding between anti-phosphotyrosine IgG and the surface-immobilized phosphopeptide (p-Src-tide) slowed the dynamic reorganization of the LC such that the system did not achieve uniform anchoring within experimentally accessible time scales (Figure 5B). This report suggests that the measurement of line defect densities and relaxation times of LCs can be used as a means to quantify areal densities of surface immobilized peptides and also to report protein binding events at such interfaces [47].

Whereas the studies described above address changes in the orientations of LCs that are triggered by the capture of targeted proteins via binding groups presented at surfaces, more recent studies have demonstrated that measurement of the anchoring energies of LCs at surfaces offers a highly sensitive and quantitative method to report the presence of captured proteins. For example, Govindaraju et al. [39] utilized such anchoring energy measurements to quantify proteins captured on surfaces decorated with oligopeptides. The presence of bound antibody caused the anchoring energy (W) of 5CB to decrease systematically from 4.4 to 1.4 $\mu J/m^2$ as the antibody concentration increased from 10 pM to 100 nM (Figure 6). Over the same range of experimental conditions, ellipsometry was not sufficiently sensitive to permit detection of the captured antibody [39].

Finally, we comment that LCs can be combined with affinity contact printing to report the presence of proteins captured on surfaces. As an example of this approach, Lowe et al. [48] covalently functionalized polydimethylsiloxane (PDMS) stamps with an antibody to the trans-membrane protein called epidermal growth factor receptor (EGFR). The anti-EGFR functionalized PDMS stamps were then used to capture EGFR and transfer it to amino-tetra(ethylene glycol)-terminated alkanethiol (EG4N) functionalized gold films by affinity contact printing. The EGFR printed onto these surfaces changed the orientation of the LC through a decrease in the anchoring energy. These effects were proposed to be the result of the presence of EGFR on the surface masking interactions between the EG4N SAM and the 5CB. The researchers demonstrated that mass densities of EGFR as low as 30-40 pg/mm^2 could be detected using the above mentioned method [48, 49].

2.2 Oligopeptides

The preceding section describes the use of LCs to report the presence of macromolecular biomolecules (i.e. proteins) at surfaces. Additionally, LCs can be used to detect the presence and state of small biomolecules displayed at surfaces. This point is illustrated in this section by describing LC ordering on surfaces presenting oligopeptides. Here we also note that, although LCs can report proteins on surfaces, the complexity of proteins has hindered identification of the intermolecular forces acting between the proteins and LCs [42, 50]. The simpler structure of oligopeptides as compared to full proteins, as well as the ability to make systematic modifications to oligopeptide structure and stereochemistry has led to fundamental insight into the intermolecular interactions underlying the ordering of LCs at biomolecular interfaces [42].

We refer the reader elsewhere for a detailed description of the anchoring of LCs on surfaces decorated with oligopepides such as IYGEFKKKC (which is a substrate for Src kinase protein, reported above) [51] and focus here on insights that have emerged from studies of the orientations of LCs on surfaces decorated with dipeptides possessing different chirality ($_{L}$-C-$_{L}$-Y vs. $_{L}$-C-$_{D}$-Y vs. $_{D}$-C-$_{D}$-Y) and phosphorylation status [42]. A particularly significant finding was that the ordering of nematic 5CB and TL205 on the dipeptide-decorated surfaces was influenced strongly by the chirality of the dipeptides (Figure 7). A series of experiments revealed that the influence of the chirality of the dipeptides on the LC was, at least in part, due to patterns of hydrogen bonds formed between the LCs and the surfaces (these results also hint at the fundamental origins of the above-mentioned influence of the orientations of immobilized proteins on the ordering of LCs). In addition, phosphorylation of the tyrosine residue in the dipeptides led to markedly different orientations of the LCs compared to their orientations on surfaces decorated with non-phosphorylated dipeptides. This difference between interactions of phosphorylated and non-phosphorylated dipeptides with LCs suggests a means to detect the phosphorylation state of dipeptides through measurements of the easy axis of LCs [42].

2.3 DNA

A third class of biomolecules that have been reported on surfaces using LCs is DNA. As noted above, LCs are promising probes of biomolecules on surfaces because they are sensitive to the orientational and configurational states of the biomolecules. This attribute is evident also in recent studies of the anchoring of LCs on surfaces presenting DNA. As described below, LCs have been successfully used to detect and quantify single and double stranded DNA (ssDNA and dsDNA) molecules at solid surfaces [52-54].

First, Nakata et al. [52] reported on the alignment of various achiral LCs (both nematic (MBBA) and smectic A (8CB) phases) on mechanically sheared dsDNA gels. An angular offset between the mean DNA orientation and the LC alignment was observed, the magnitude of which differed for 8CB and MBBA. Building from these observations, Malone and Schwartz [41] investigated the alignment of nematic LCs on isolated DNA molecules extended on a surface. They observed that the LC was aligned in the direction of ssDNA extension, whereas dsDNA caused alignment at an oblique angle (Figure 8), similar to that reported by Nikata et al. In contrast to Nikata et al. [52], however, this study [41]

demonstrated that the alignment of two different LCs (MBBA and 5CB) by dsDNA were the same within experimental error. Malone and Schwartz suggest these differences in LC alignment might arise from LC mesogens interacting with parts of the stretched dsDNA helix that are not accessible when the dsDNA molecules are instead organized into closely packed DNA gels. Key conclusions of their study are that LCs can be used to image DNA on surfaces at extraordinary low densities (at an area fraction occupied by DNA of 10^{-6}) and that the orientations assumed by LCs can, in principle, form the basis of sensitive sensors of DNA hybridization (i.e. indicating whether or not dsDNA or ssDNA is presented on the surface). Before ending this section, we refer the interested reader to another report of the use of LCs to detect DNA (including specific sequences) at solid surfaces [53].

3. Biomolecular sensing at LC-aqueous interfaces

Water plays a key role in preserving the structure and functionality of many biomolecules. The recent series of publications characterizing interfaces formed between thermotropic (oily) LCs and aqueous phases thus provides new opportunities to create biological sensors based on LCs [55, 56]. We begin this section by noting some key conceptual differences between LC-aqueous interfaces and the more extensively studied LC-solid interface (as described above). Specifically, we comment that (i) the LC-aqueous interface is soft and deformable relative to LC-solid interfaces, (ii) the mobility of molecules at LC-aqueous interfaces is high as compared to solid surfaces, thus enabling lateral reorganization of biomolecules upon binding to LC-aqueous interface, and (iii) the organization of molecules at LC-aqueous interfaces is influenced by the elasticity of the LC, leading to interfacial phase states of molecules that are not realized at LC-solid interfaces [57]. As illustrated below, these various attributes of LC-aqueous interfaces lead to a rich range of phenomena that promise the realization of biosensors with attributes not found in other sensing technologies.

The geometry of a typical experiment performed to report biomolecular interactions at the LC-aqueous interface is shown in Figure 9 [56]. The LC is hosted in the pores of an electron microscopy grid that is supported on a glass microscope slide treated with a self-assembled monolayer of octadecyltrichlorosilane (OTS). Immersion of the supported film of LC into an aqueous phase leads to the formation of a stable interface between the aqueous phase and LC (Figure 9A). The capture of adsorbates at this interface (typically from the aqueous phase) can trigger anchoring transitions in the LC films, resulting in a range of different orientations (Figure 9B-D) and thus optical appearances of LC films (Figure 9E-G).

3.1 Phospholipid-decorated LC-aqueous interfaces

[58, 59] The first example of biosensing at the LC-aqueous interface involves the use of phospholipids of the type found in biological membranes. In this example, aqueous suspensions of dilaurylphosphatidylcholine (DLPC) in the form of small unilamellar vesicles were placed into contact with a film of LC. Fusion of the vesicles with the interface of the LC triggered the anchoring of 5CB at the interface to change discontinuously from a planar to homeotropic orientation (Figure 10A-C). The density of lipid present on the LC-aqueous interface was subsequently characterized using quantitative epifluorescence microscopy and it was found that at saturation coverage, a monolayer of DLPC was

adsorbed at the interface (0.45nm^2/ molecule). Fluorescence recovery after photobleaching (FRAP) experiments also revealed that the phospholipids at the interface were laterally mobile, exhibiting diffusion coefficients that were comparable to those measured within lipid bilayers. The homeotropic orientation assumed by the LC at the lipid-decorated interface was interpreted to be due to molecular interdigitation of the tails of the phospholipids and the mesogens forming the LC, a conclusion that is supported by a number of early studies on the interactions of LCs and lipids supported on solid surfaces (Langmuir-Blodgett films of lipids) [60].

Lipid-decorated LC-aqueous interfaces, as described above, were used by Brake and co-workers to report protein binding and enzymatic events [61]. Brake showed that both specific binding interactions between the enzyme phospholipase A_2 and lipids, as well as subsequent enzymatic hydrolysis of the lipids (binding and/or hydrolysis), led to the reorganization of the lipids in a manner that was optically reported as a dynamic orientational transition in the LC. In contrast, non-specific interactions between proteins (e.g. albumin, lysozyme, and cytochrome-*c*) and the lipid-laden interface of the LC did not trigger orientational transitions in the LCs. When reporting enzymatic hydrolysis of the lipids, concurrent epifluorescence and polarized light imaging of the lipids and proteins labelled with fluorophores at the LC-aqueous interface showed that spatially patterned orientations of the LCs reflected the lateral organization (micrometer-sized domains) of the proteins and lipids, respectively, at the LC-aqueous interface (Figure 10D-H). Closely related to this observation, beta-bungarotoxin, which exhibits Ca^{2+}-dependent phospholipase A_2 activity, has also been shown to induce an anchoring transition in the LC when it hydrolyzed a phospholipid monolayer assembled at the LC-aqueous interface [62]. The selectivity was demonstrated by the lack of response of the phospholipid-decorated LC to alpha-bungarotoxin and myotoxin II, both of which do not exhibit any phospholipase activity.

Whereas the examples above involve specific interactions between lipids and proteins at the LC interface, we note also that the LC-aqueous interface provides an opportunity to report the interactions between biomolecules that are non-specific in nature. For example, De Tercero et al. [63] reported on non-specific interactions of proteins with LC-aqueous interfaces decorated with *partial* monolayer coverage of DLPC. Whereas non-specific interactions of four proteins (cytochrome c, bovine serum albumin, immunoglobulins, and neutravidin) do not perturb the ordering of the LC when a *full* monolayer of DLPC is assembled at the LC-aqueous interface, patterned orientations of the LC that reflect penetration and subsequent lateral organization of proteins into the interface of the LC were observed with *partial* monolayer coverage of DLPC. The shapes of the protein domains in the lipid layer (ellipsoidal domains in the case of BSA or elongated networks in the case of IgGs) hint at the relative strength and directionality of the lipid-lipid, lipid-protein and protein-protein interactions at these interfaces. These results indicate that phospholipid-decorated interfaces formed between LC and aqueous phases offer the basis of a simple tool with which to study the spatial organization and dynamics of protein networks formed at mobile, lipid-decorated interfaces.

We note also the use of phospholipid-decorated LC-aqueous interfaces to report non-specific interactions involving protein-coated nanoparticles [64]. This approach was motivated by the goal of providing new methods to assess the potential cytotoxicity of nanomaterials, where interactions between nanoparticles and cell membranes are thought, in some cases, to underlie cytotoxicity. In these studies, it was observed that interactions between protein-coated gold nanoparticles (AuNPs) and phospholipid monolayers assembled at LC-aqueous interfaces triggered orientational transitions of the LCs.

Finally, we comment that LC-aqueous interfaces have also been used to report the interaction of cationic anti-microbial peptides with anionic lipids [65]. Prior to contact with the antimicrobial peptides, the LC interfaces decorated with the anionic lipids exhibited homeotropic orientations. However, bright domains were observed in the LC (corresponding to tilted orientations of the LC) when antimicrobial peptides were introduced into the aqueous phase. In contrast, no change in the optical appearance of the LC was reported (i.e. a homeotropic orientation was maintained) when antimicrobial peptides were incubated against an LC interface presenting a monolayer of zwitterionic phospholipids. The LC anchoring transition observed in the presence of the anionic lipid and antimicrobial peptide was interpreted to be due to formation of a complex between the two species at the interface of the LC. This approach hints at the potential utility of LCs in studies of membrane disruption or permeabilization caused by antimicrobial agents.

In the examples described above, the phospholipids were fused spontaneously with the aqueous interface of the LCs, a result of so-called hydrophobic interactions between LC and the phospholipids. In additional studies, s*pecific* capture of ligand-functionalized phospholipid vesicles has been reported at LC-aqueous interfaces that were decorated with a monolayer of adsorbed protein (streptavidin or anti-biotin antibody) (Figure 11A) [66]. The specific binding of the vesicles to the proteins was demonstrated to trigger a continuous anchoring transition (continuous change in the tilt) in the LC, which was quantified by measurement of the optical retardance of the LC (Figure 11B-D). The observation of a continuous change in the ordering of the LC contrasts with prior reports of fusion of lipid vesicles with protein-free interfaces of LCs, where discontinuous transitions and the appearance of micrometer-sized domains of lipid were observed. This difference was interpreted to indicate that the presence of the protein on the interface limits the size of lipid domains to the sub-optical range, resulting in a far-field tilt of the LC (which changes with the fraction of the interface decorated with lipids and proteins). Overall, these results demonstrate that LC ordering transitions have the potential to be useful for reporting specific binding events involving vesicles and proteins. Here we note that detection and quantification of microvesicles shed by cells is an area of growing significance in biology and medicine because analysis of the microvesicles can provide information about the states of the cells.

3.2 Molecules tailored for biosensing at the LC-aqueous interface

The examples presented above reveal that a key challenge underlying the use of LC-aqueous interfaces for biosensing is the functionalization of the interface of the LC such that anchoring transitions of the LCs are triggered by a targeted biomolecular interaction.

Whereas phospholipids have proved effective for that purpose, an opportunity exists to functionalize LC-aqueous interfaces with non-natural molecules that present biologically-relevant chemical functionality and thereby cause the LC to undergo well-defined anchoring transitions in the presence of targeted analytes. Below we summarize several recent studies that have tailored the interfacial properties of LCs using synthetic and semi-synthetic molecules.

The first example addresses the use of conjugates formed between synthetic surfactants and oligopeptides, and the interaction of these conjugates with enzymes [67, 68]. Park and Abbott showed that oligopeptide-decorated interfaces of LCs can be prepared by covalently attaching an oligopeptide (with 17 amino-acid residues) to the terminal carboxylic acid groups of surfactants adsorbed at the aqueous interface of the LC (Figure 12A). Conjugation of the oligopeptides to the surfactants led to an anchoring transition in the LC due to the reorganization of the monolayer. In contrast, physical adsorption of oligopeptides onto the surfactant-laden interface of the LC did not cause an anchoring transition, thus highlighting the role of covalent bond formation. Significantly, the authors also demonstrated that introduction of a protease, which catalysed the hydrolysis of the oligopeptide-surfactant conjugate, released the surfactants from the oligopeptide-induced organization, thus resulting in an anchoring transition that returned the LC to the orientation exhibited prior to conjugate with the oligopeptide (Figure 12B-C). This result suggests that oligopeptide-decorated LCs provide a convenient and simple method to selectively report protease activity.

As a second example of the design of a synthetic modifier of LC interfaces, we briefly mention the use of nitrilotriacetic acid-terminated amphiphiles. When adsorbed at LC-aqueous interfaces and primed with Ni^{2+} ions, these amphiphiles were used to bind histidine-tagged ubiquitin through binding of the Ni^{2+} to the histidine tag [69]. When the LC interfaces presenting immobilized histidine-tagged ubiquitin were exposed to an aqueous solution of anti-ubiquitin antibody, an orientational transition was induced in the LC, presumably also due to a change in organization of the amphiphiles at the interface.

A third example involves the use of LC interfaces decorated with cationic surfactants to report hybridization of oligonucleotides [70-72]. This approach builds from past studies that have demonstrated that cationic amphiphiles form organized assemblies with DNA in bulk solution [70-72]. Whereas a complex formed between octadecyltrimethylammoniurn bromide (OTAB) and single-stranded DNA (ssDNA) at the aqueous interface of nematic 5CB caused a tilted orientation of the LC, exposure of the ssDNA/OTAB interfacial complex to its ssDNA complement resulted in the nucleation, growth, and coalescence of regions that caused homeotropic LC alignment (Figure 12E). Fluorescence microscopy revealed that the complement was co-localized in the same regions as the homeotropic domains, and that exposure to non-complementary ssDNA caused no such response. These results support the conclusion that the homeotropic regions were due to DNA hybridization.

Finally, we comment that block copolymers containing liquid crystalline blocks (LCP) are an additional class of molecules that have been used to functionalize interfaces of LCs for detection of proteins [73, 74]. Although this approach appears promising, to date, however,

the detection of proteins has been non-selective. For example, Seo et al. [74] adsorbed an amphiphilic block copolymer of PAA-*b*-LCP and demonstrated that adsorption of several different proteins in the μM-range caused a transition from homeotropic to planar anchoring of 5CB. These authors also demonstrated that they could detect proteins in human urine from a patient having albuminuria (with a detection limit of 0.032 mg/mL).

3.3 pH-based biosensors.

Many enzymatic events lead to the consumption or generation of a proton, and thus detection of pH is a common method to detect enzymatic activity. Building from this observation, a series of studies have reported the design of pH-sensitive LC-aqueous interfaces for the purpose of reporting enzymatic activities that lead to changes in pH.

As first example, we comment that it has been reported that 5CB, when doped with *4′-pentyl-biphenyl-4-carboxylic acid (PBA)*, undergoes an anchoring transition in response to protonation and deprotonation of PBA at the LC-aqueous interface. Building from this observation, the PBA-doped LC was used to monitor local pH changes triggered by enzymatic reactions. As a proof of concept, the hydrolysis of penicillin G by surface-immobilized penicillinase was reported through a pH-induced anchoring transition [75]. A second example involves the detection of catalase activity based on doping of the aldehyde dodecanal into 5CB. In brief, hydrogen peroxide was generated by the catalytic oxidation of dodecanal into dodecanoic acid, thus leading to homeotropic anchoring as the dodecanoic acid formed carboxylate anions at the aqueous interface [76]. Finally, we note that urease has been detected via changes in pH that were induced by the reaction product ammonia [77]. This method was successfully used to detect urease belonging to the family of amidohydrolase, which hydrolyzes urea into ammonia and carbon dioxide. This ammonia-based LC biosensor may be useful for sensitive detection of other amidohydrolases.

3.4 Tailored mesogens for biosensing

Finally, we note that a largely untapped opportunity exists to design mesogens tailored for biosensing at the LC-aqueous interface. As a first step in this direction, mesogens have been designed containing oligomeric ethylene glycol (Figure 12D) [78]. The approach was inspired by past studies that have demonstrated that monolayers of oligomeric ethylene glycol can passivate surfaces to strong, non-specific adsorption of proteins. To explore if a similar strategy could be used at the surface of an LC film, miscible mixtures of 5CB and EG4-LC (a mesogen with a tetra(ethylene glycol) tail) were contacted with an aqueous phase. LC mixtures containing 1-5% wt/wt of EG4-LC triggered an anchoring transition to a homeotropic orientation, consistent with partitioning of EG4-LC from the bulk of the LC to its aqueous interface. Significantly, the interfacial partitioning of the EG4-LC also lowered the level of non-specific adsorption of BSA to the interface of the LC. Minimization of non-specific adsorption of proteins to the interfaces of synthetic materials represents a key challenge in the design of biotic–abiotic interface. The results demonstrate a general and facile approach to the design of LC interfaces that present biologically relevant chemical functional groups, exhibit well-defined anchoring at aqueous interfaces, and exhibit minimal non-specific adsorption of proteins.

4. LC-in-water emulsions as sensors

Whereas the sensors described above employ LC confined to planar films with thicknesses of several micrometers, droplets of LC dispersed in water (i.e. LC-in-water emulsions) are rapidly emerging as promising candidates for LC-based sensing. Specifically, LC emulsions have now been utilized to report the presence of surfactants [79-81], lipids [79, 82-84], charged macromolecules [85], bacteria [86], viruses [86], and proteins [79, 87] in aqueous solution.

In many of the past studies that have employed LC emulsions as sensors, a target analyte adsorbs to the surfaces of the LC droplets, triggering a change in the surface anchoring of the LC and thus the configuration of the LC within the droplet (Figure 13). Recent studies of LC emulsion-based sensors have been motivated by several advantages that they offer relative to sensors based on planar films of LC (described above). First, in contrast to the sensors based on planar films of LC, sensors based on LC emulsions do not require surface treatment of solid substrates to define the initial orientation of the LC [88]. Instead, the initial director configuration within the droplets of an LC emulsion is defined by the chemistry of the droplet interfaces. Second, as will be discussed in detail below, the ordering of the LC confined within the droplets of LC emulsions is sensitive to the size of the droplets, thus providing an additional means to tune the response of the LC droplets to the presence of target analytes or changes to bulk solution conditions (i.e. by controlling the size of the droplets) [80, 89]. Finally, droplets contained in LC emulsions are highly mobile, thereby providing advantages in terms of sample handling (e.g. using microfluidics), reagent mixing, and detection [90].

4.1 Preparation of LC-in-water emulsions

Emulsion droplets can be prepared by various techniques, such as photopolymerization [91], ultrasonication [92], shearing of droplets and subsequent crystallization fractionation [93, 94], droplet break-off in a co-flowing stream (microfluidics) [95], and dispersion polymerization [91, 96, 97]. However, the majority of these methods do not permit control over LC droplet size in the range that is optimal for LC sensing (1-10 μm, see below). To address this need, Sivakumar et al. [98] demonstrated that monodisperse emulsions can be prepared through the templating of polyelectrolyte multilayer capsules. Figure 14 illustrates this method of preparation of emulsions. The process is initiated by layer-by-layer deposition of polymers (e.g. poly(sodium-4-styrene sulfonate) (PSS) and poly(allylamine hydrochloride) (PAH)) onto the surfaces of silica templates dispersed in aqueous solution. After deposition of the polymeric layers, the silica cores are selectively etched, and the resulting capsules are filled with low molecular weight LC. The major advantages of the templating process are that the size of the LC droplets can be controlled by selection of the size of the silica template, and the interfacial chemistry of the LC droplets can be controlled by selection of the types of polymers. More recently, Khan et al. used a microfluidic device to fabricate monodisperse emulsions of microdroplets decorated with an amphiphilic block copolymer [90], although the sizes of the LC droplets contained in these emulsions were large (~ 30 μm). Whereas microfluidic approaches are limited to droplet production rates on the order of 1000 s^{-1} [90, 99], the templating process described above is highly scalable.

4.2 Sensing with LC droplets using adsorbate-induced ordering transitions

LC emulsions can be used to detect the presence of a variety of target analytes in solution. As mentioned above, in one approach, the target analyte adsorbs to the surface of the LC droplets, causing a change in the anchoring energy of the LC in the droplets. As the first example, Gupta et al. [79] characterized water-dispersed 5CB droplets undergoing a bipolar-to-radial ordering transition in response to increasing concentrations of sodium dodecyl sulfate (SDS) (Figure 15). The transition began with the disappearance of the two point defects (boojums) at the diametric ends of the bipolar droplet and the appearance of a disclination near the droplet equator. As the alignment changed from parallel to perpendicular, this ring defect moved towards a pole and shrank to a surface point defect. Finally, the point defect migrated from the surface of the droplet to the center, forming a radial structure. Here we comment that this series of topological states is similar to that reported by Volovik and Lavrentovich [83] in studies of the effects of temperature on glycerol-dispersed 5CB droplets in the presence of lecithin, but different from that reported by Prischepa et al. [82], who characterized the ordering within 5CB droplets suspended in a poly(vinyl butyral) matrix in response to increasing bulk concentrations of lecithin.

Whereas the results above clearly demonstrate that LC droplets can be used to detect synthetic amphiphiles, recent studies have also demonstrated that LC droplets can be used as a basis of sensors for important biological lipids. Specifically, Lin et al. [84] demonstrated that pg/mL concentrations of endotoxin can trigger bipolar-to-radial ordering transitions within micrometer-sized droplets of 5CB dispersed in an aqueous medium (Figure 16). Significantly, these concentrations are five orders of magnitude lower than that required to drive ordering transitions via a uniform adsorbate-induced change in the surface anchoring energies of the droplets. A series of experiments reported by Lin et al. support the proposal that the transitions are driven, instead, by self-association of endotoxin at the sites of topological defects present in the LC droplets. In addition, they demonstrate the response of the LC droplets (percentage of LC droplets exhibiting a radial configuration) to the presence of a fixed concentration of endotoxin can be tuned by controlling the number of droplets present in solution (Figure 16G). For example, in a solution containing 10 pg/mL endotoxin, when ~8,300 droplets were present ~80% of the droplets exhibited a radial configuration. In contrast, when ~94,000 droplets are present Figure 16G predicts that ~25% of the droplets should exhibit a radial configuration.

Finally, we comment that Bera and Fang [85] showed that polyelectrolyte-coated LC droplets can be used to detect charged macromolecules in solution. Adsorption of positively charged dendrimers on negatively charged polyelectrolyte-coated droplets caused bipolar-to-radial ordering transitions, which were dependent on both the size and number of droplets present in solution. This study serves to highlight the complexity of interfacial phenomena that occurs in these LC-in-water emulsion systems.

4.3 Detection of biomolecules using LC droplets

LC droplets dispersed in water, when decorated with a range of synthetic and biological molecules, have been shown to enable several schemes for the detection of proteins, bacteria and viruses. The first example that we discuss uses LC droplets decorated with

phospholipids. Analogous to the above-described sensor based on a planar film of 5CB decorated with a monolayer of L-DLPC utilized by Brake et al. [59, 61] to report the enzymatic activity of phospholipase A_2 (Figure 10), Gupta et al. [79] demonstrated that aqueous dispersions of 5CB droplets coated with a monolayer of the phospholipid L-DLPC can also be used to report the enzymatic activity of phospholipase A_2. After the enzyme cleaved an aliphatic tail from L-DLPC, the lyso-lipid spontaneously desorbed from the LC-aqueous interface and entered the bulk aqueous phase. The enzymatic processing of the lipid resulted in a radial-to-bipolar ordering transition within the LC droplets.

More recently, Alino et al. [87] demonstrated that antibody-decorated LC droplets dispersed in aqueous solutions can be utilized for immunoassays. In their system, polyethylenimine (PEI)-coated LC droplets were treated with glutaraldehyde (GA) to provide aldehyde groups for immobilization of the antibody human immunoglobulin G (IgG) on the surface of the droplets. The IgG-coated LC droplets were suspended in a phosphate buffered saline (PBS) solution containing the surfactant Tween 20. The authors demonstrated that the presence of Tween 20 induced a bipolar-to-radial ordering transition within the droplets, and proposed that the amphiphilic nature of Tween 20 allows it to permeate through the IgG-coated PEI layer and concentrate on the surface of the LC droplets. This mechanism is similar to the mechanism proposed by Gupta et al., where the amphiphilic nature of SDS allows it to permeate through polyelectrolyte multilayers (PEMs) on PEM-coated LC droplets to induce an ordering transition within the droplets via an adsorbate-induced change in the anchoring energy of the droplets [79, 80]. After IgG was immobilized on the surface of the PEI-coated LC droplets, the droplets were incubated in a PBS-Tween 20 solution containing the antigen anti-IgG. Through the use of a fluorescently labelled version of anti-IgG, it was demonstrated that binding of anti-IgG to IgG results in a radial-to-bipolar ordering transition within the LC droplets. The authors proposed that due to its large size, the immunocomplex is able to displace some Tween 20 from the surface of the LC droplets resulting in the observed radial-to-bipolar ordering transition. Additional investigations are needed to explore further this proposition.

While the two examples described above serve to illustrate the opportunity that LC droplets present for biosensing, several past studies provide general guidance for optimization of future designs of biosensors based on LC droplets. Here we summarize some of these key observations. First, by using the above-described polymer templating method to fabricate water-dispersed PEM-coated 5CB droplets of a controlled size, Gupta et al. [80] demonstrated that decreasing the size of the LC droplets led to spontaneous bipolar-to-radial ordering transitions below a critical droplet diameter of approximately 800 nm ($R \approx 400$ nm) (Figure 17C-M). Although many theoretical scaling arguments predicted the size-dependent stability of director configurations within LC droplets [92, 100, 101], these arguments generally predict a spontaneous transition to a uniform director configuration within sub-micrometer sized LC droplets (Figure 17A and B) rather than a transition to the radial configuration. Gupta et al. [80] also showed that the sensitivity of LC droplets which undergo a bipolar-to-radial ordering transition in the presence of interfacial adsorbates can be adjusted by controlling the size of the droplets (Figure 17N). In addition to droplet size, the sensitivity of LC droplets to interfacial adsorbates can be tuned by manipulating the solution conditions of the confining phase. For example, Khan et al. [90] demonstrated that

monodisperse emulsions of microdroplets decorated with an amphiphilic block copolymer are sensitive to changes in the pH of the bulk aqueous phase, as a change in pH from 12 to 2 led to radial-to-bipolar ordering transitions. Similarly, Zou et al. [102] showed that 5CB droplets coated with multilayers of poly(styrenesulfonate sodium (PSS) and poly(diallyldimethylammonium chloride) (PDADMAC) undergo radial-to-bipolar ordering transitions upon increasing the bulk concentration of sodium chloride (NaCl). While droplet size and the conditions of the confining solution can be manipulated to adjust the sensitivity of LC droplets to the presence of interfacial adsorbates, the response time of the droplets can be controlled by tailoring the chemistry of the droplet interface. This was illustrated by a study conducted by Tjipto et al. [81] showing that PEM coatings on LC droplets slowed surfactant-induced bipolar-to-radial ordering transitions by two orders of magnitude relative to bare LC droplets. Additionally, it was demonstrated that polymer-coated droplets can be immobilized on chemically functionalized surfaces, which could form a platform for high-throughput screening of different solutions, although the nature of the surfaces must be controlled as certain surface chemistries can led to ordering transitions within the droplets upon immobilization [88].

Finally, we comment that, as will be discussed further below, Sivakumar et al. [86] showed that monodisperse LC droplets can detect and distinguish between different types of bacteria and viruses. Whereas gram-negative bacteria and enveloped viruses were able to trigger a bipolar-to-radial ordering transition within the droplets, gram-positive bacteria and non-enveloped viruses did not lead to an ordering transition. We refer the reader to the section below for a detailed description of these studies.

5. LCs as sensors of viruses, bacteria and mammalian cells

As discussed above, past studies have shown that interactions between phospholipids and mesogens of LC phases can trigger LC orientational transitions. Because many viruses, bacteria as well as mammalian cells are encapsulated by lipid membranes, recent studies have been performed to investigate their interactions with LCs. These studies have demonstrated that contact between LCs and lipid-encapsulated viruses [86, 103, 104] and gram-negative bacteria [86, 105] can drive ordering transitions within the LC, implicating LCs as potentially useful sensors of these virions and microorganisms. This is a promising capability, as the rapid and sensitive detection of harmful microorganisms and infectious agents is important for upholding public health and safety in areas including food processing, water and environmental monitoring, and clinical diagnostics [106]. Additionally, several studies have investigated the impact that contact with various LCs has on the viability of cells [107-109] and microorganisms [109, 110]. In particular, it was found that LC interfaces can be used to support the growth of cells [111, 112]. Such LC-based substrates may have utility in reporting interactions with cells. In the following section, we detail the progress that has been made in understanding the interactions between viruses, bacteria, and mammalian cells with LCs.

5.1 Viruses

Espinoza et al. [103] first demonstrated that LCs can be utilized for the detection of lipid-encapsulated viruses. Solutions of vesicular stomatitis virus (VSV) were incubated on the

surface of gold slides treated with poly-L-lysine. Electrostatic attractions between the VSV outer membrane and the polycation film led to immobilization of the VSV at the surface. Next, LC optical cells were created by sandwiching 5CB between the VSV-decorated slides and reference slides which induced homeotropic anchoring. It was shown that interactions between the LCs and the VSV-treated surface induced homeotropic LC ordering when a critical density of the virus was captured on the slide.

Jang et al. [104] extended the study described above by examining the LC anchoring properties of surfaces treated with additional viruses besides VSV, including adenovirus, influenza, and La Crosse virus. It was discovered that only surfaces upon which sufficient densities of lipid-encapsulated viruses were captured induced homeotropic anchoring of a contacting LC film (Figure 18). Adenovirus, which lacks an outer lipid envelope, did not give rise to homeotropic anchoring at any virus concentration tested. Thus, the authors proposed that physical interaction between the lipid envelope of viruses and the LC was responsible for giving rise to the homeotropic alignment of 5CB.

As discussed in the preceding section of this review, LC emulsion droplets have been employed recently for a variety of sensing applications. For example, it has been shown that, following the transfer and assembly of a monolayer of lipids at the LC-aqueous interface, LC droplets undergo a bipolar-to-radial ordering transition. Sivakumar et al. [86] exploited this phenomenon in extending the use of these LC droplets to the detection and differentiation of various strains of viruses in aqueous solutions. It was demonstrated that incubation of LC droplets with a lipid-encapsulated virus, *A/NWS/Tokyo/67*, gave rise to the bipolar-to-radial ordering transition. This likely occurred following adsorption of viral lipids at the LC-aqueous interface. No such transition was observed following incubation of droplets with *M13 helper phage*, a non-enveloped virus. The divergent responses of the LC droplets to these two viruses suggest another means through which lipid-encapsulated viral strains can be differentiated from non-enveloped strains.

5.2 Bacteria

In addition to viruses, Sivakumar et al. [86] explored the interactions between LC droplets and various bacterial strains. Bacteria are generally classified as either gram-negative or gram-positive based on the presence or absence, respectively, of an outer lipid membrane. The study found that, when a solution containing gram-negative bacteria, such as *E. coli*, was added to the LC emulsion, transfer of membrane lipids was observed to drive a bipolar-to-radial ordering transition in the droplets (Figure 19A and B). No such transition, however, occurred following incubation of droplets with a gram-positive bacterium, *B. subtilis* (Figure 19C and D).

5.3 Mammalian cells

Before discussing experimental results that demonstrate that LCs can be used as engineered materials that support the attachment and growth of mammalian cells, we comment first on enabling studies that were performed to identify thermotropic LCs with limited toxicity towards living cells. Specifically, Luk et al. [107] found that although 5CB and several other LCs exhibited toxicity when added above cultures of mammalian cells (3T3 fibroblasts and

corneal epithelial cells), LCs containing fluorocarbon functionalities, including TL205 and the C-series (see Figure 20A), did not cause pronounced cell death. In a subsequent study performed by Lockwood et al. [108], 5CB was found to partition to a much greater extent than TL205 into multi-lamellar DPPC vesicles, which served as simple models for cell membranes (Figure 20B). The authors suggested that the physical mechanisms behind the dissimilar partitioning of TL205 and 5CB into the DPPC bilayers might also underlie the observed difference in toxicity of cells contacted with 5CB and TL205.

Additional studies have investigated the compatibility of various lyotropic LCs with cells. Specifically, Cheng et al. [109] reported that contact with the lyotropic LC disodium cromoglycate (DSCG) is not toxic to human epitheloid cervical carcinoma (HeLa) cells. Also, it was shown that VSV can still successfully infect HeLa cells in the presence of the DSCG. Woolverton et al. [110] additionally found that various species of bacteria remained viable following suspension within volumes of four different lyotropic chromonic LCs (Neutral Grey, Red 14, Blue 27, and DSCG). Following the identification of particular LCs which are not toxic to mammalian cells, subsequent reports demonstrated successful use of LC substrates for the attachment and proliferation of mammalian cells. Lockwood et al. [111] found that human embryonic stem cells (hESCs) can survive and grow on a protein (Matrigel)-decorated LC-aqueous interface in which TL205 was used as the LC (Figure 21A). Cell-driven reorganization of the Matrigel layer was observed over the course of a week, which allowed regions of the TL205 film to come into contact with the aqueous cell media. The LC at this interface adopted a homeotropic orientation, which was concluded to be a consequence of the adsorption of lipids present in the cell media solution onto the LC-media interface (see Figure 21).

Agarwal et al. [112] found that cells such as fibroblasts, in contrast to hESCs, were unable to grow at the LC-aqueous interface (Figure 22A and B). This was attributed to the fact that fibroblasts require more rigid substrates for successful attachment and growth. The investigators found that instead, an LC composite material, a colloid-in-LC (CLC) gel, could be successfully utilized as a substrate for fibroblast growth (Figure 22C and D). The LC domains within these CLC gels were shown to still be responsive to changes in surface anchoring, suggesting these gels could also potentially be exploited in the future for reporting biomolecular interactions with the LC.

In summary, LCs have been successfully used to sense and detect bacteria and viruses. Additionally, non-toxic LCs have been identified and utilized for supporting the growth of mammalian cells and for reporting interfacial cell-protein interactions. This research, when combined, shows that LCs are promising candidates for use in these biological contexts. A number of questions, however, remain to be addressed. For example, there exists a great diversity of lipids within the membranes of bacteria, viruses, and cells. Tail length, multiplicity, and degree of unsaturation, in addition to lipid phase behaviour, can all vary greatly amongst biological lipids. There remains an incomplete understanding of how all of these parameters impact the way in which these lipids organize at the LC interface and impact the ordering of the LC. Also, biological buffers and media are fairly complex and typically include salts, proteins and lipids; all of which may also influence the ordering of

LC films. Thus, given this complex environment, the challenge is to design LC interfaces that respond solely to the biological targets of interest.

Conclusion

The range of examples presented in this review demonstrates that surface-induced ordering of LCs can be exploited in diverse contexts to create LC-based sensors of chemical and biological species. The fundamental challenge, which is common to all of the studies reported in this paper, is that of understanding how the structure and organization of molecules at LC interfaces impacts the ordering of LCs. While this challenge has been addressed in the context of development of LC-based technologies for displays, the diversity and complexity of the interfaces that form the basis of chemical and biological sensors far exceeds that encountered in electrooptical devices such as LC displays. In some examples presented in this paper, such as the use of LCs for chemical sensors, substantial progress has been made in understanding the molecular interactions responsible for the functioning of the sensor. For example, IR spectroscopic evidence supports the central role of metal ion-ligand coordination interactions in controlling the orientation of LCs in sensors for organophosphonate-based compounds (e.g., nerve agents). However, in many of the other examples described in this review, our understanding of the molecular-level interactions responsible for the functioning of the sensors remains to be fully developed. This is particularly true of LC-based sensors of biological molecules. For example, whereas LC-based methods for reporting proteins show substantial promise (e.g. reporting antibody-antigen interactions), the underlying intermolecular interactions responsible for the changes measured in anchoring energies of LCs on protein-decorated surfaces have not been identified. The use of small fragments of proteins (oligopeptides) has, in recent studies, provided the basis of some useful insights (e.g. role of chirality and hydrogen bonding), and additional studies in this direction will likely yield additional knowledge that will permit, in the long term, rational design of LC interfaces for biological sensing.

The examples described in this review also highlight the potential utility of interfaces formed between aqueous phases and thermotropic LCs for biological sensing. Whereas a great deal of past effort has been devoted to understanding the orientational ordering of LCs at the surfaces of solids, aqueous interfaces of LCs are fundamentally different from LC-solid interfaces in that they are soft and deformable interfaces, at which interfacial adsorbates exhibit high lateral mobility, and where the elasticity of the LC can drive the organization of adsorbates. In this respect, the LC is not a passive reporter of the presence of targeted analytes at its interface, but rather the LC participates in directing the formation of interfacial assemblies of relevance to biological sensing. For example, elastic stresses in LCs can lead to the concentration of assemblies of adsorbates at localized regions in LCs, which in turn trigger changes in the ordering of the LC. This fundamental phenomenon underlies, for example, the sensitivity and selectivity of the response of LC droplets (dispersed in water) to endotoxin.

Acknowledgments

This work was primarily supported by NSF through DMR-1121288 (Materials Research Science and Engineering Center), the Army Research Office (W911NF-11-1-0251 and W911NF-10-1-0181), and the National Institutes of

Health (CA108467, CA105730 and 5T32GM08349.). Acknowledgment of support is also made to the Department of Energy, Basic Energy Sciences, Biomaterials Program (DESC0004025).

References

1. Fréedericksz, V.; Repiewa, A. Zeitschrift für Physik A Hadrons and Nuclei. Vol. 42. German: 1927. Theoretisches und Experimentelles zur Frage nach der Natur der anisotropen Flüssigkeiten [Theoretical and experimental work on the question of the nature of anisotropic fluids].; p. 532-546.
2. Fréedericksz V, Zolina V. Forces causing the orientation of an anisotropic liquid. Trans Faraday Soc. 1933; 29:919–930.
3. Kawamoto H. The history of liquid-crystal displays. Proc IEEE. 2002; 90:460–500.
4. Gray GW, Kelly SM. Liquid crystals for twisted nematic display devices. J Mater Chem. 1999; 9:2037–2050.
5. Schadt M. Liquid crystal materials and liquid crystal displays. Annu Rev Mater Sci. 1997; 27:305–379.
6. Goodby JW. The nanoscale engineering of nematic liquid crystals for displays. Liq Cryst. 2011; 38:1363–1387.
7. Clark MG, Harrison KJ, Raynes EP. Liquid-crystal materials and devices. Phys Technol. 1980; 11:232–240.
8. Ohm C, Brehmer M, Zentel R. Liquid crystalline elastomers as actuators and sensors. Adv Mater. 2010; 22:3366–3387. [PubMed: 20512812]
9. Marcos C, Pena JMS, Torres JC, Santos JI. Temperature-frequency converter using a liquid crystal cell as a sensing element. Sensors. 2012; 12:3204–3214. [PubMed: 22737002]
10. Herzer N, Guneysu H, Davies DJD, Yildirim D, Vaccaro AR, Broer DJ, et al. Printable optical sensors based on H-bonded supramolecular cholesteric liquid crystal networks. J Am Chem Soc. 2012; 134:7608–7611. [PubMed: 22519954]
11. Chatterjee S, Anna SL. Formation and ordering of topological defect arrays produced by dilatational strain and shear flow in smectic-A liquid crystals. Phys Rev E: Stat, Nonlinear, Soft Matter Phys. 2012; 85:011701.
12. Chanishvili A, Chilaya G, Petriashvili G, Barberi R, Bartolino R, De Santo MP. Cholesteric liquid crystal mixtures sensitive to different ranges of solar UV irradiation. Mol Cryst Liquid Cryst. 2005; 434:353–366.
13. Wang Y, Li Q. Light-driven chiral molecular switches or motors in liquid crystals. Adv Mater. 2012; 24:1926–1945. [PubMed: 22411073]
14. Sutarlie L, Yang KL. Monitoring spatial distribution of ethanol in microfluidic channels by using a thin layer of cholesteric liquid crystal. Lab Chip. 2011; 11:4093–4098. [PubMed: 22030694]
15. Saha A, Tanaka Y, Han Y, Bastiaansen CMW, Broer DJ, Sijbesma RP. Irreversible visual sensing of humidity using a cholesteric liquid crystal. Chem Commun. 2012; 48:4579–4581.
16. Winterbottom DA, Narayanaswamy R, Raimundo IM. Cholesteric liquid crystals for detection of organic vapours. Sens Actuators, B. 2003; 90:52–57.
17. Dickert FL, Haunschild A, Hofmann P. Cholesteric liquid crystals for solvent vapour detection — Elimination of cross sensitivity by band shape analysis and pattern recognition. Fresenius' J Anal Chem. 1994; 350:577–581.
18. Poziomek EJ, Novak TJ, Mackay RA. Use of liquid crystals as vapor detectors. Mol Cryst Liquid Cryst. 1974; 27:175–185.
19. Sutarlie L, Qin H, Yang KL. Polymer stabilized cholesteric liquid crystal arrays for detecting vaporous amines. Analyst. 2010; 135:1691–1696. [PubMed: 20583347]
20. Kirchner N, Zedler L, Mayerhofer TG, Mohr GJ. Functional liquid crystal films selectively recognize amine vapours and simultaneously change their colour. Chem Commun. 2006; (14): 1512–1514.
21. Shah RR, Abbott NL. Coupling of the orientations of liquid crystals to electrical double layers formed by the dissociation of surface-immobilized salts. J Phys Chem B. 2001; 105:4936–4950.

22. Carlton RJ, Gupta JK, Swift CL, Abbott NL. Influence of simple electrolytes on the orientational ordering of thermotropic liquid crystals at aqueous interfaces. Langmuir. 2012; 28:31–36. [PubMed: 22106820]
23. Yang ZQ, Abbott NL. Spontaneous formation of water droplets at oil-solid interfaces. Langmuir. 2010; 26:13797–13804. [PubMed: 20712383]
24. Stewart, CE. Weapons of mass casualties and terrorism response handbook: Jones & Bartlett Learning. 2006.
25. Cantalini C, Valentini L, Armentano I, Lozzi L, Kenny JM, Santucci S. Sensitivity to NO_2 and cross-sensitivity analysis to NH_3, ethanol and humidity of carbon nanotubes thin film prepared by PECVD. Sens Actuators, B. 2003; 95:195–202.
26. Shah RR, Abbott NL. Principles for measurement of chemical exposure based on recognition-driven anchoring transitions in liquid crystals. Science. 2001; 293:1296–1299. [PubMed: 11509724]
27. Yang KL, Cadwell K, Abbott NL. Mechanistic study of the anchoring behavior of liquid crystals supported on metal salts and their orientational responses to dimethyl methylphosphonate. J Phys Chem B. 2004; 108:20180–20186.
28. Yang KL, Cadwell K, Abbott NL. Use of self-assembled monolayers, metal ions and smectic liquid crystals to detect organophosphonates. Sens Actuators, B. 2005; 104:50–56.
29. Wang PH, Yu JH, Zhao YB, Li ZJ, Li GQ. A novel liquid crystal-based sensor for the real-time identification of organophosphonate vapors. Sens Actuators, B. 2011; 160:929–935.
30. Cadwell KD, Lockwood NA, Nellis BA, Alf ME, Willis CR, Abbott NL. Detection of organophosphorous nerve agents using liquid crystals supported on chemically functionalized surfaces. Sens Actuators, B. 2007; 128:91–98.
31. Shah RR, Abbott NL. Orientational transitions of liquid crystals driven by binding of organoamines to carboxylic acids presented at surfaces with nanometer-scale topography. Langmuir. 2003; 19:275–284.
32. Bi X, Yang KL. Real-time liquid crystal-based glutaraldehyde sensor. Sens Actuators, B. 2008; 134:432–437.
33. Xu H, Bi X, Ngo X, Yang K-L. Principles of detecting vaporous thiols using liquid crystals and metal ion microarrays. Analyst. 2009; 134:911–915. [PubMed: 19381384]
34. Cadwell KD, Alf ME, Abbott NL. Infrared spectroscopy of competitive interactions between liquid crystals, metal salts, and dimethyl methylphosphonate at surfaces. J Phys Chem B. 2006; 110:26081–26088. [PubMed: 17181261]
35. Pal SK, Acevedo-Vélez C, Hunter JT, Abbott NL. Effects of divalent ligand interactions on surface-induced ordering of liquid crystals. Chem Mater. 2010; 22:5474–5482.
36. Hunter JT, Pal SK, Abbott NL. Adsorbate-induced ordering transitions of nematic liquid crystals on surfaces decorated with aluminum perchlorate salts. ACS Appl Mater Interfaces. 2010; 2:1857–1865.
37. Bungabong ML, Ong PB, Yang KL. Using copper perchlorate doped liquid crystals for the detection of organophosphonate vapor. Sens Actuators, B. 2010; 148:420–426.
38. Luk YY, Yang KL, Cadwell K, Abbott NL. Deciphering the interactions between liquid crystals and chemically functionalized surfaces: Role of hydrogen bonding on orientations of liquid crystals. Surf Sci. 2004; 570:43–56.
39. Govindaraju T, Bertics PJ, Raines RT, Abbott NL. Using measurements of anchoring energies of liquid crystals on surfaces to quantify proteins captured by immobilized ligands. J Am Chem Soc. 2007; 129:11223–11231. [PubMed: 17705384]
40. Gupta VK, Skaife JJ, Dubrovsky TB, Abbott NL. Optical amplification of ligand-receptor binding using liquid crystals. Science. 1998; 279:2077–2080. [PubMed: 9516101]
41. Malone SM, Schwartz DK. Macroscopic liquid crystal response to isolated DNA helices. Langmuir. 2011; 27:11767–11772. [PubMed: 21894894]
42. Bai YQ, Abbott NL. Enantiomeric interactions between liquid crystals and organized monolayers of tyrosine-containing dipeptides. J Am Chem Soc. 2012; 134:548–558. [PubMed: 22091988]

43. Jang CH, Tingey ML, Korpi NL, Wiepz GJ, Schiller JH, Bertics PJ, et al. Using liquid crystals to report membrane proteins captured by affinity microcontact printing from cell lysates and membrane extracts. J Am Chem Soc. 2005; 127:8912–8913. [PubMed: 15969543]
44. Skaife JJ, Abbott NL. Quantitative interpretation of the optical textures of liquid crystals caused by specific binding of immunoglobulins to surface-bound antigens. Langmuir. 2000; 16:3529–3536.
45. Skaife JJ, Abbott NL. Influence of molecular-level interactions on the orientations of liquid crystals supported on nanostructured surfaces presenting specifically bound proteins. Langmuir. 2001; 17:5595–5604.
46. Luk YY, Tingey ML, Dickson KA, Raines RT, Abbott NL. Imaging the binding ability of proteins immobilized on surfaces with different orientations by using liquid crystals. J Am Chem Soc. 2004; 126:9024–9032. [PubMed: 15264835]
47. Clare BH, Abbott NL. Orientations of nematic liquid crystals on surfaces presenting controlled densities of peptides: Amplification of protein-peptide binding events. Langmuir. 2005; 21:6451–6461. [PubMed: 15982053]
48. Lowe AM, Ozer BH, Bai YQ, Bertics PJ, Abbott NL. Design of surfaces for liquid crystal-based bioanalytical assays. ACS Appl Mater Interfaces. 2010; 2:722–731. [PubMed: 20356273]
49. Lowe AM, Bertics PJ, Abbott NL. Quantitative methods based on twisted nematic liquid crystals for mapping surfaces patterned with bio/chemical functionality relevant to bioanalytical assays. Anal Chem. 2008; 80:2637–2645. [PubMed: 18355089]
50. Tingey ML, Snodgrass EJ, Abbott NL. Patterned orientations of liquid crystals on affinity microcontact printed proteins. Adv Mater. 2004; 16:1331–1336.
51. Clare BH, Guzman O, de Pablo J, Abbott NL. Anchoring energies of liquid crystals measured on surfaces presenting oligopeptides. Langmuir. 2006; 22:7776–7782. [PubMed: 16922563]
52. Nakata M, Zanchetta G, Buscaglia M, Bellini T, Clark NA. Liquid crystal alignment on a chiral surface: Interfacial interaction with sheared DNA films. Langmuir. 2008; 24:10390–10394. [PubMed: 18489190]
53. Chen CH, Yang KL. Detection and quantification of DNA adsorbed on solid surfaces by using liquid crystals. Langmuir. 2010; 26:1427–1430. [PubMed: 19961190]
54. Lai SL, Tan WL, Yang KL. Detection of DNA targets hybridized to solid surfaces using optical images of liquid crystals. ACS Appl Mater Interfaces. 2011; 3:3389–3395. [PubMed: 21861457]
55. Brake JM, Abbott NL. An experimental system for imaging the reversible adsorption of amphiphiles at aqueous-liquid crystal interfaces. Langmuir. 2002; 18:6101–6109.
56. Lockwood NA, Gupta JK, Abbott NL. Self-assembly of amphiphiles, polymers and proteins at interfaces between thermotropic liquid crystals and aqueous phases. Surf Sci Rep. 2008; 63:255–293.
57. Gupta JK, Meli MV, Teren S, Abbott NL. Elastic energy-driven phase separation of phospholipid monolayers at the nematic liquid-crystal-aqueous interface. Phys Rev Lett. 2008; 100:048301. [PubMed: 18352339]
58. Brake JM, Daschner MK, Abbott NL. Formation and characterization of phospholipid monolayers spontaneously assembled at interfaces between aqueous phases and thermotropic liquid crystals. Langmuir. 2005; 21:2218–2228. [PubMed: 15752009]
59. Brake JM, Daschner MK, Luk YY, Abbott NL. Biomolecular interactions at phospholipid-decorated surfaces of liquid crystals. Science. 2003; 302:2094–2097. [PubMed: 14684814]
60. Hiltrop K, Stegemeyer H. Alignment of liquid-crystals by amphiphilic monolayers. Ber Bunsen-Ges Phys Chem Chem Phys. 1978; 82:884–889.
61. Brake JM, Abbott NL. Coupling of the orientations of thermotropic liquid crystals to protein binding events at lipid-decorated interfaces. Langmuir. 2007; 23:8497–8507. [PubMed: 17595119]
62. Hartono D, Lai SL, Yang KL, Yung LYL. A liquid crystal-based sensor for real-time and label-free identification of phospholipase-like toxins and their inhibitors. Biosens Bioelectron. 2009; 24:2289–2293. [PubMed: 19162466]
63. De Tercero MD, Abbott NL. Ordering transitions in liquid crystals permit imaging of spatial and temporal patterns formed by proteins penetrating into lipid-laden interfaces. Chem Eng Commun. 2008; 196:234–251. [PubMed: 23671353]

64. Hartono D, Qin WJ, Yang KL, Yung LYL. Imaging the disruption of phospholipid monolayer by protein-coated nanoparticles using ordering transitions of liquid crystals. Biomaterials. 2009; 30:843–849. [PubMed: 19027155]
65. Hu QZ, Jang CH. Using liquid crystals to report molecular interactions between cationic antimicrobial peptides and lipid membranes. Analyst. 2012; 137:567–570. [PubMed: 22108758]
66. Tan LN, Orler VJ, Abbott NL. Ordering transitions triggered by specific binding of vesicles to protein-decorated interfaces of thermotropic liquid crystals. Langmuir. 2012; 28:6364–6376. [PubMed: 22372743]
67. Park JS, Abbott NL. Ordering transitions in thermotropic liquid crystals induced by the interfacial assembly and enzymatic processing of oligopeptide amphiphiles. Adv Mater. 2008; 20:1185–1190.
68. Hu QZ, Jang CH. Liquid crystal-based imaging of enzymatic reactions at aqueous-liquid crystal interfaces decorated with oligopeptide amphiphiles. Bull Korean Chem Soc. 2010; 31:1262–1266.
69. Hartono D, Xue CY, Yang KL, Yung LYL. Decorating liquid crystal surfaces with proteins for real time detection of specific protein-protein binding. Adv Funct Mater. 2009; 19:3574–3579.
70. McUmber AC, Noonan PS, Schwartz DK. Surfactant-DNA interactions at the liquid crystal-aqueous interface. Soft Matter. 2012; 8:4335–4342.
71. Price AD, Schwartz DK. DNA hybridization-induced reorientation of liquid crystal anchoring at the nematic liquid crystal/aqueous interface. J Am Chem Soc. 2008; 130:8188–8194. [PubMed: 18528984]
72. Lai SL, Hartono D, Yang KL. Self-assembly of cholesterol DNA at liquid crystal/aqueous interface and its application for DNA detection. Appl Phys Lett. 2009; 95:153702.
73. Park JS, Teren S, Tepp WH, Beebe DJ, Johnson EA, Abbott NL. Formation of oligopeptide-based polymeric membranes at interfaces between aqueous phases and thermotropic liquid crystals. Chem Mater. 2006; 18:6147–6151.
74. Seo JM, Khan W, Park SY. Protein detection using aqueous/LC interfaces decorated with a novel polyacrylic acid block liquid crystalline polymer. Soft Matter. 2012; 8:198–203.
75. Bi X, Hartono D, Yang KL. Real time liquid crystal pH sensor for monitoring enzymatic activities of penicillinase. Adv Funct Mater. 2009; 19:3760–3765.
76. Hu QZ, Jang CH. Using liquid crystals for the label-free detection of catalase at aqueous-LC interfaces. J Biotechnol. 2012; 157:223–227. [PubMed: 22138010]
77. Hu QZ, Jang CH. Using liquid crystals for the real-time detection of urease at aqueous/liquid crystal interfaces. J Mater Sci. 2012; 47:969–975.
78. Yang Z, Gupta JK, Kishimoto K, Shoji Y, Kato T, Abbott NL. Design of biomolecular interfaces using liquid crystals containing oligomeric ethylene glycol. Adv Funct Mater. 2010; 20:2098–2106. [PubMed: 22199989]
79. Gupta JK, Zimmerman JS, de Pablo JJ, Caruso F, Abbott NL. Characterization of adsorbate-induced ordering transitions of liquid crystals within monodisperse droplets. Langmuir. 2009; 25:9016–9024. [PubMed: 19719217]
80. Gupta JK, Sivakumar S, Caruso F, Abbott NL. Size-dependent ordering of liquid crystals observed in polymeric capsules with micrometer and smaller diameter. Angew Chem Int Ed. 2009; 48:1652–1655.
81. Tjipto E, Cadwell KD, Quinn JF, Johnston APR, Abbott NL, Caruso F. Tailoring the interfaces between nematic liquid crystal emulsions and aqueous phases via layer-by-layer assembly. Nano Lett. 2006; 6:2243–2248. [PubMed: 17034091]
82. Prischepa OO, Shabanov AV, Zyryanov VY. Transformation of director configuration upon changing boundary conditions in droplets of nematic liquid crystal. JETP Lett. 2004; 79:257–261.
83. Volovik GE, Lavrentovich OD. The topological dynamics of defects - boojums in nematic drops. Zh Eksp Teor Fiz. 1983; 85:1997–2010.
84. Lin IH, Miller DS, Bertics PJ, Murphy CJ, de Pablo JJ, Abbott NL. Endotoxin-induced structural transformations in liquid crystalline droplets. Science. 2011; 332:1297–1300. [PubMed: 21596951]
85. Bera T, Fang JY. Polyelectrolyte-coated liquid crystal droplets for detecting charged macromolecules. J Mater Chem. 2012; 22:6807–6812.

86. Sivakumar S, Wark KL, Gupta JK, Abbott NL, Caruso F. Liquid crystal emulsions as the basis of biological sensors for the optical detection of bacteria and viruses. Adv Funct Mater. 2009; 19:2260–2265.
87. Alino VJ, Pang J, Yang KL. Liquid crystal droplets as a hosting and sensing platform for developing immunoassays. Langmuir. 2011; 27:11784–11789. [PubMed: 21863867]
88. Kinsinger MI, Buck ME, Abbott NL, Lynn DM. Immobilization of polymer-decorated liquid crystal droplets on chemically tailored surfaces. Langmuir. 2010; 26:10234–10242. [PubMed: 20405867]
89. Zou JH, Fang JY. Director configuration of liquid-crystal droplets encapsulated by polyelectrolytes. Langmuir. 2010; 26:7025–7028. [PubMed: 20000598]
90. Khan W, Choi JH, Kim GM, Park SY. Microfluidic formation of pH responsive 5CB droplets decorated with PAA-b-LCP. Lab Chip. 2011; 11:3493–3498. [PubMed: 21874196]
91. Vennes M, Zentel R. Liquid-crystalline colloidal particles. Macromol Chem Phys. 2004; 205:2303–2311.
92. Tixier T, Heppenstall-Butler M, Terentjev EM. Spontaneous size selection in cholesteric and nematic emulsions. Langmuir. 2006; 22:2365–2370. [PubMed: 16489830]
93. Bibette J. Depletion interactions and fractionated crystallization for polydisperse emulsion purification. J Colloid Interface Sci. 1991; 147:474–478.
94. Hsu P, Poulin P, Weitz DA. Rotational diffusion of monodisperse liquid crystal droplets. J Colloid Interface Sci. 1998; 200:182–184.
95. Fernandez-Nieves A, Cristobal G, Garces-Chavez V, Spalding GC, Dholakia K, Weitz DA. Optically anisotropic colloids of controllable shape. Adv Mater. 2005; 17:680–684.
96. Sandomirski K, Martin S, Maret G, Stark H, Gisler T. Highly birefringent colloidal particles for tracer studies. J Phys: Condens Matter. 2004; 16:S4137–S4144.
97. Vennes M, Martin S, Gisler T, Zentel R. Anisotropic particles from LC polymers for optical manipulation. Macromolecules. 2006; 39:8326–8333.
98. Sivakumar S, Gupta JK, Abbott NL, Caruso F. Monodisperse emulsions through templating polyelectrolyte multilayer capsules. Chem Mater. 2008; 20:2063–2065.
99. Xu S, Nie Z, Seo M, Lewis P, Kumacheva E, Stone H, et al. Generation of monodisperse particles by using microfluidics: Control over size, shape, and composition. Angew Chem Int Ed. 2005; 44:724–728.
100. Drzaic, PS. Liquid crystal dispersions. World Scientific; Singapore ; River Edge, NJ: 1995.
101. Lavrentovich OD. Topological defects in dispersed liquid crystals, or words and worlds around liquid crystal drops. Liq Cryst. 1998; 24:117–125.
102. Zou JH, Bera T, Davis AA, Liang WL, Fang JY. Director configuration transitions of polyelectrolyte coated liquid-crystal droplets. J Phys Chem B. 2011; 115:8970–8974. [PubMed: 21667976]
103. Espinoza LAT, Schumann KR, Luk YY, Israel BA, Abbott NL. Orientational behavior of thermotropic liquid crystals on surfaces presenting electrostatically bound vesicular stomatitis virus. Langmuir. 2004; 20:2375–2385. [PubMed: 15835699]
104. Jang CH, Cheng LL, Olsen CW, Abbott NL. Anchoring of nematic liquid crystals on viruses with different envelope structures. Nano Lett. 2006; 6:1053–1058. [PubMed: 16683850]
105. Xu H, Hartono D, Yang KL. Detecting and differentiating Escherichia coli strain TOP10 using optical textures of liquid crystals. Liq Cryst. 2010; 37:1269–1274.
106. Lazcka O, Del Campo FJ, Muñoz FX. Pathogen detection: a perspective of traditional methods and biosensors. Biosens Bioelectron. 2007; 22:1205–1217. [PubMed: 16934970]
107. Luk YY, Campbell SF, Abbott NL, Murphy CJ. Non-toxic thermotropic liquid crystals for use with mammalian cells. Liq Cryst. 2004; 31:611–621.
108. Lockwood NA, Meli MV, Surjosantoso A, Kim EB, de Pablo JJ, Abbott NL. Characterization of the interactions between synthetic nematic LCs and model cell membranes. Liq Cryst. 2007; 34:1387–1396.

109. Cheng LL, Luk YY, Murphy CJ, Israel BA, Abbott NL. Compatibility of lyotropic liquid crystals with viruses and mammalian cells that support the replication of viruses. Biomaterials. 2005; 26:7173–7182. [PubMed: 15955554]

110. Woolverton CJ, Gustely E, Li L, Lavrentovich OD. Liquid crystal effects on bacterial viability. Liq Cryst. 2005; 32:417–423.

111. Lockwood NA, Mohr JC, Ji L, Murphy CJ, Palecek SP, de Pablo JJ, et al. Thermotropic liquid crystals as substrates for imaging the reorganization of matrigel by human embryonic stem cells. Adv Funct Mater. 2006; 16:618–624.

112. Agarwal A, Huang E, Palecek S, Abbott NL. Optically responsive and mechanically tunable colloid-in-liquid crystal gels that support growth of fibroblasts. Adv Mater. 2008; 20:4804–4809.

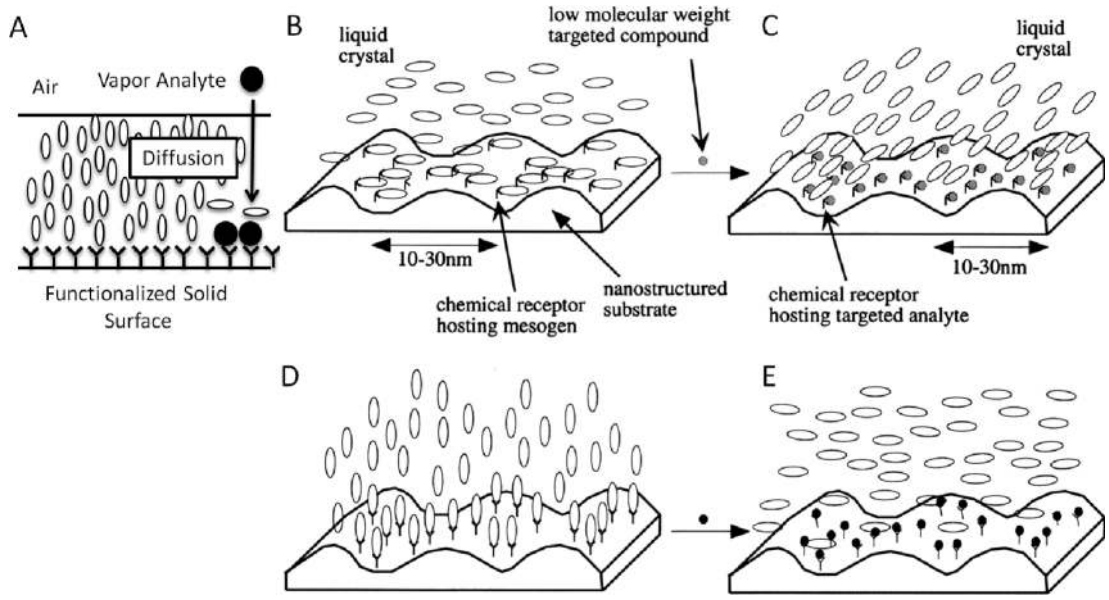

Figure 1.

(A) Schematic illustration of LC-based sensor. A thin film of LC is exposed to air containing an analyte that diffuses across the LC film and binds with the solid surface to change the anchoring of the LC. (B, C) A schematic illustration of an LC sensor for the detection of organoamines from a gas phase. The initial alignment of nematic 5CB supported on a carboxylic acid-terminated SAM is perpendicular to the anisotropic grooves of the solid substrate, as shown in (B). In the presence of organoamines that bind with the carboxylic acid groups on the surface more favorably than nematic 5CB, the orientation of the 5CB is dictated by the topography of the surface (resulting in an azimuthal alignment along the anisotropic grooves) (C). (D, E) A schematic illustration of an LC sensor that detects organophosphonate molecules. Prior to exposure to the analyte, the interaction of nematic 5CB with the copper perchlorate-decorated surfaces aligns the LC homeotropically, as shown in (D). The homeotropic orientation of the 5CB is lost in the presence of an organophosphonate (E). Reproduced with permission [26].

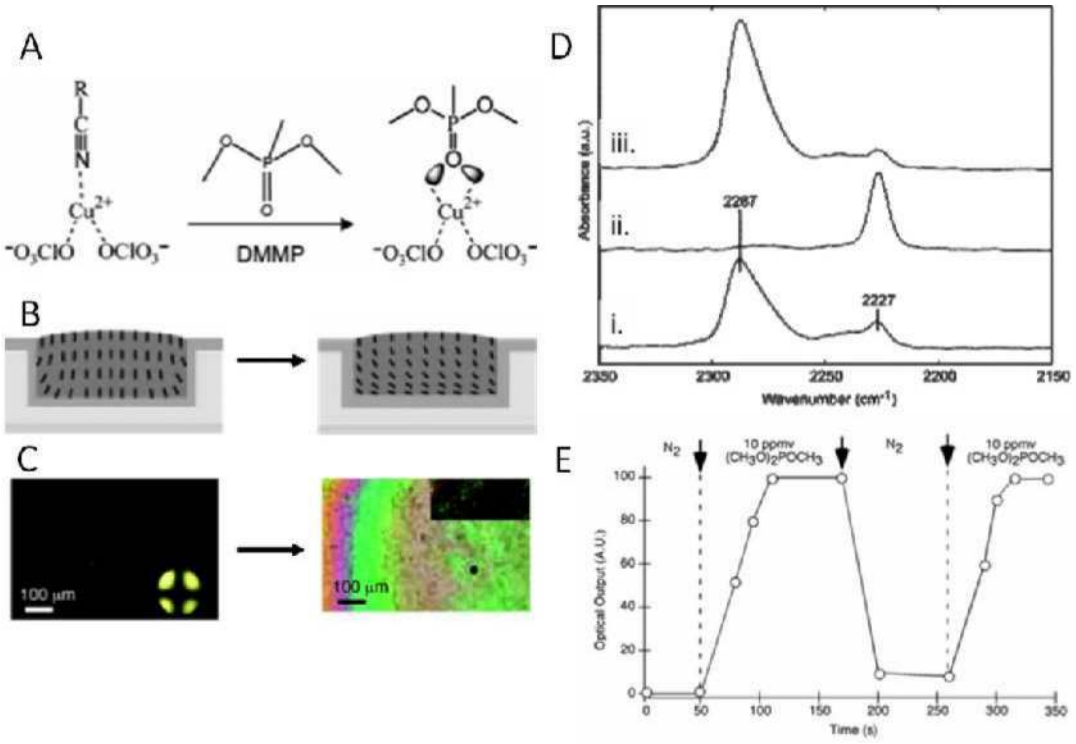

Figure 2.

(A) Schematic illustration of DMMP-triggered disruption of a coordination interaction between the nitrile group of 5CB and the copper (II) perchlorate. (B) Illustration of the orientation of nematic 5CB in a microwell, before and after the ligand exchange depicted in (A). The copper (II) perchlorate is deposited on the bottom of the well. (C) Optical micrographs (crossed polarisers) of micrometer-thick films of 5CB supported on copper (II) perchlorate before (left) and after (right) exposure to DMMP. (D) PM-IRRAS spectrum corresponding to the nitrile stretch vibration (i) in the presence of air, (ii) in the presence of 10 ppm DMMP, (iii) after a 30 min purge of DMMP by air (see text for details). (E) The optical response of the thin films of 5CB exposed sequentially to nitrogen and 10 ppm DMMP. Reproduced with permission [26, 34].

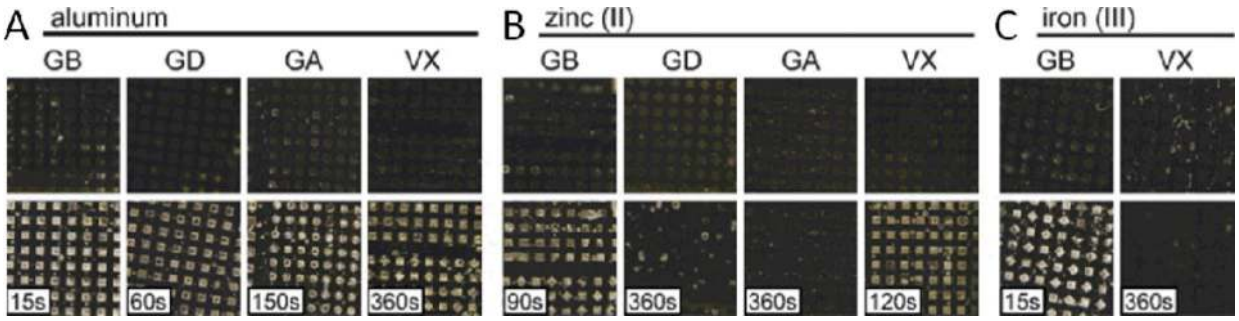

Figure 3.

Optical micrographs (crossed polarisers) of nematic E7 supported within microwells containing perchlorate salts of (A) aluminum, (B) zinc (II), and (C) iron (III), before (top row) and after (bottom row) exposure to organophosphonate nerve agents (GB – sarin, GD –soman, GA – tabun, and VX). The duration of exposure is indicated. The images areas are approximately 7.5 mm by 7.5 mm. Reproduced with permission [30].

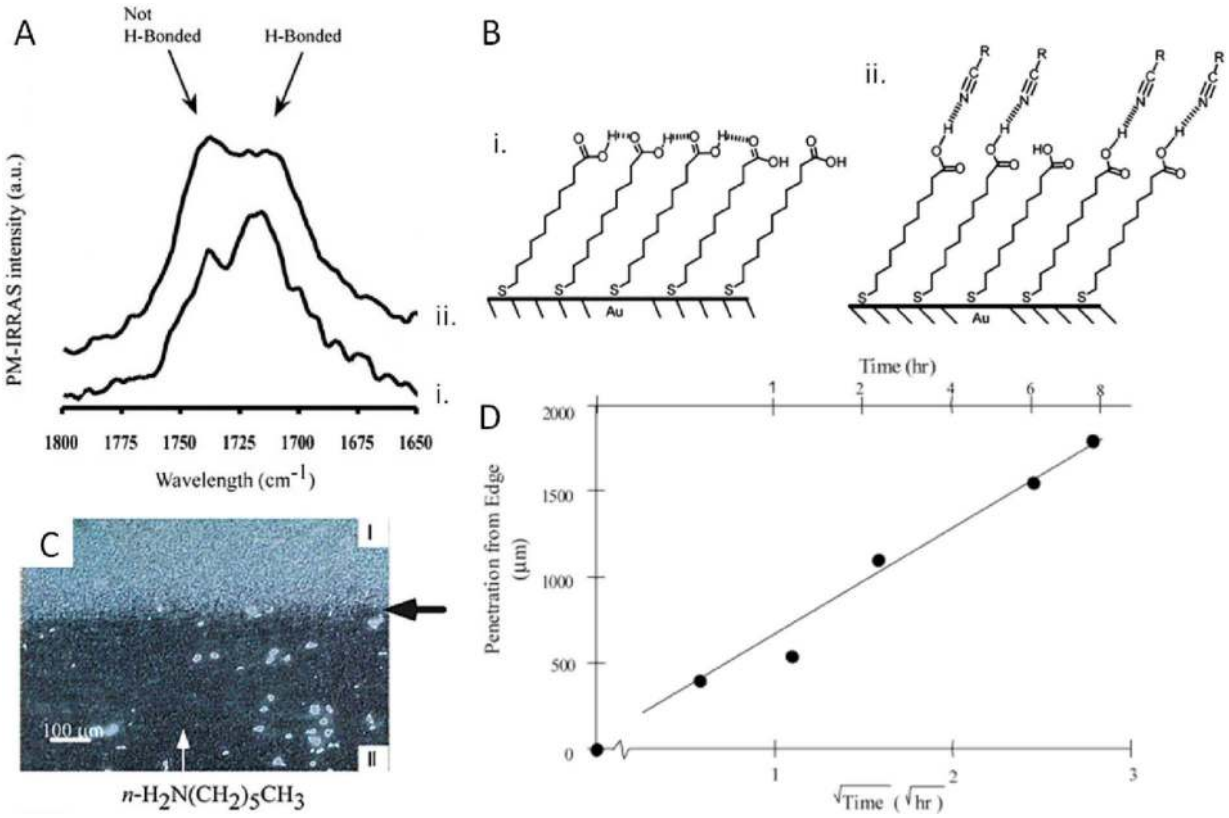

Figure 4.

(A) PM-IRRAS spectra of carboxylic-acid terminated SAMs (i) before and (ii) after contact with 8CB. (B) Schematic illustration of hydrogen bonding within a carboxylic acid-terminated SAM before (left) and after (right) contact with 8CB. (C) An optical image (between cross polarisers) of LC cell (thickness ~12 μm) with surfaces formed from carboxylic acid-terminated SAMs. The edge of the cell was exposed to 750 ppm of n-$H_2N(CH_2)_5CH_3$. In region I, the presentation of the carboxylic acid on the surface (and hydrogen bonding with the LC) causes a twist distortion of the LC. However, in the presence of the amine in region II, the LC relaxes to the azimuthal alignment of the film dictated by the anisotropic topography of the surface. (D) The penetration distance (from the open edge of the LC cell) of n-$H_2N(CH_2)_5CH_3$ plotted as a function of the square root of exposure time. Reproduced with permission [31, 38].

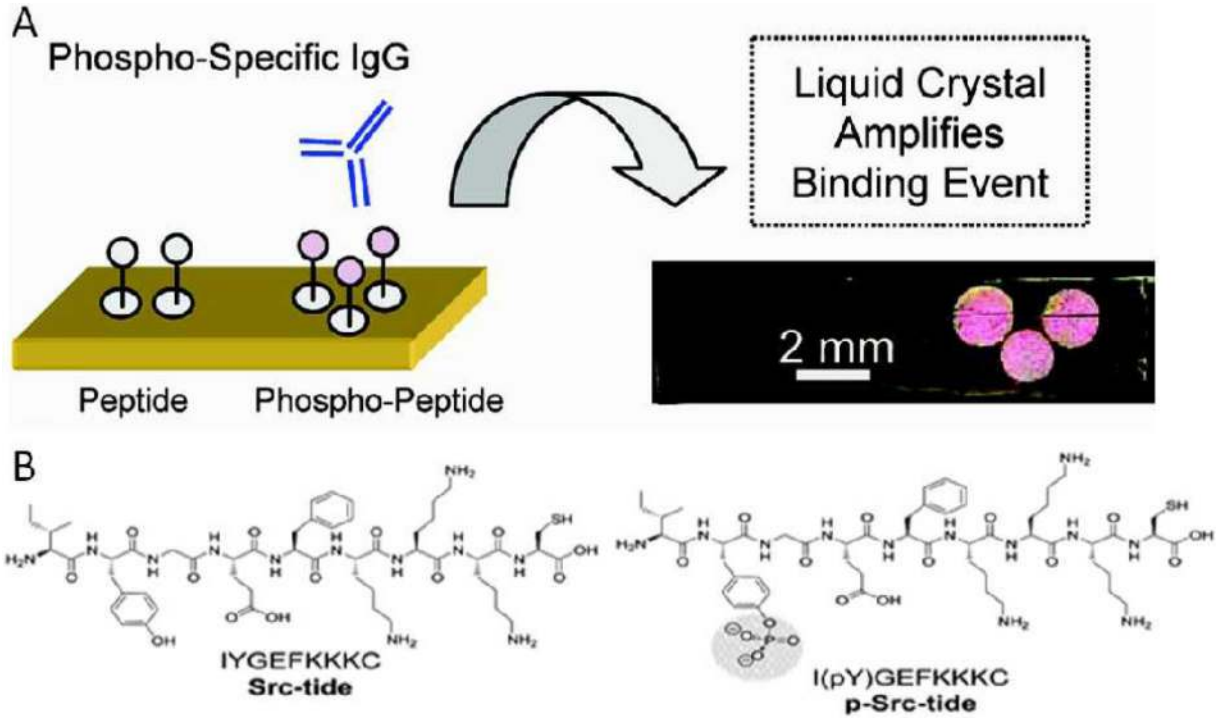

Figure 5.

(A) Schematic illustration and optical images (polarised light microscopy) demonstrating the use of LCs to amplify and report protein binding events occurring on a spatially resolved peptide array. (B) Optimized peptide substrate of the Src kinase protein and synthetic peptide equivalent to the phosphorylated peptide product after Src kinase modification. Reproduced with permission [47].

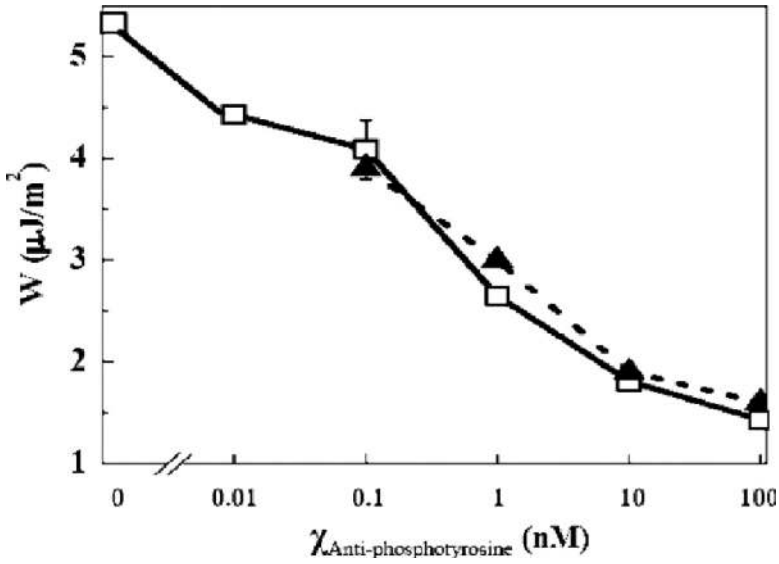

Figure 6.

Plot of anchoring energy (W) of nematic LC (5CB) on an oligopeptide-presenting surface as a function of the solution concentration of monoclonal anti-phosphotyrosine antibody (IgG) that was incubated with the surface before LC cell assembly. Two independent data sets are shown with a standard error calculated from five repeat measurements at 100 pM antibody. Reproduced with permission [39].

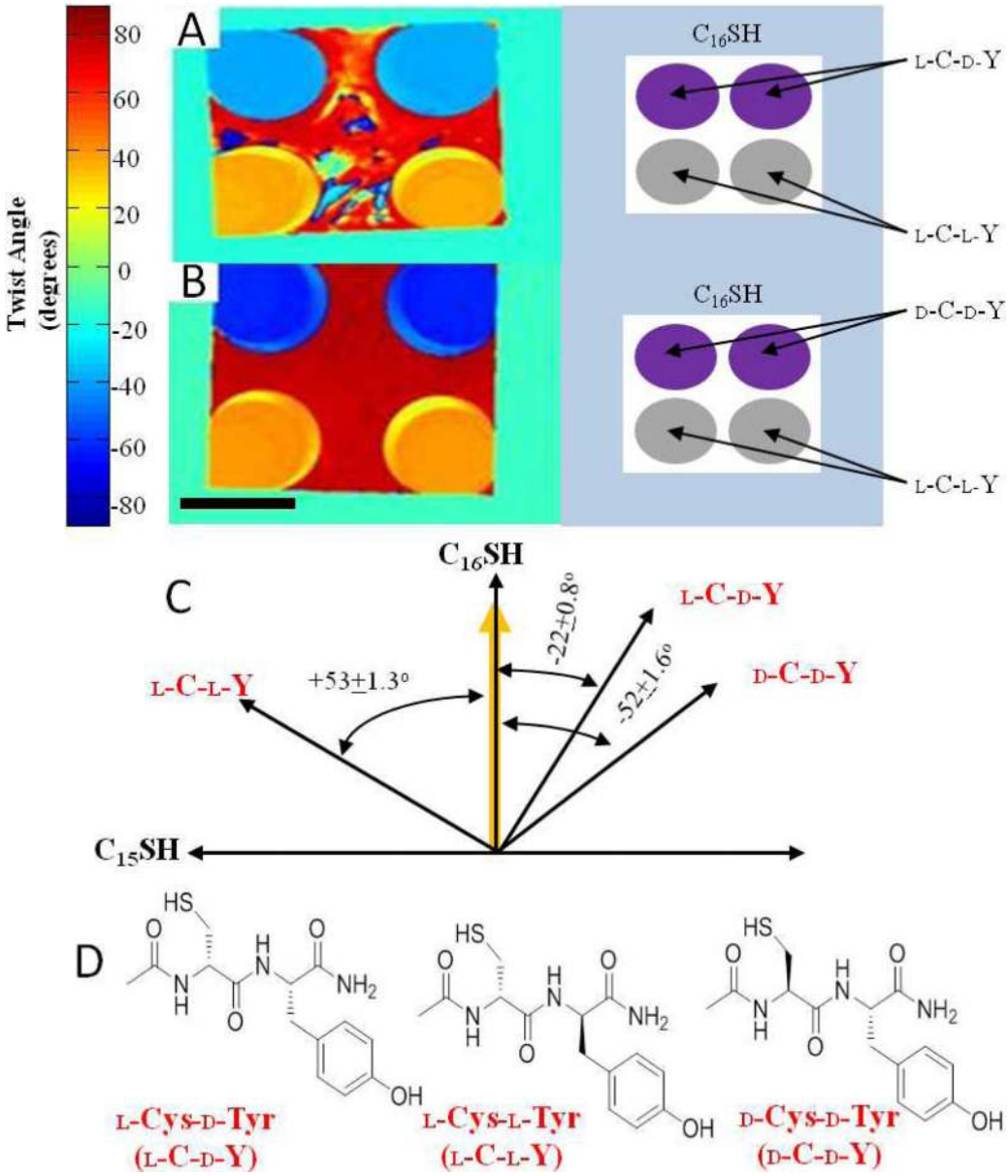

Figure 7.

(A) Map of twist angles of nematic 5CB on gold films decorated with monolayers of L-C-D-Y or L-C-L-Y. (B) Map of twist angles of nematic 5CB on gold films decorated with monolayers of D-C-D-Y or L-C-L-Y. The scale bar is 2 mm. (C) Angle diagram and quantitative analysis of the easy axes of 5CB on L-C-L-Y, L-C-D-Y-, and D-C-D-Y-decorated surfaces relative to the direction of gold deposition (yellow arrow) and reference surfaces ($C_{15}SH$ and $C_{16}SH$). (D) Chemical structures of these dipeptides. Reproduced with permission [42].

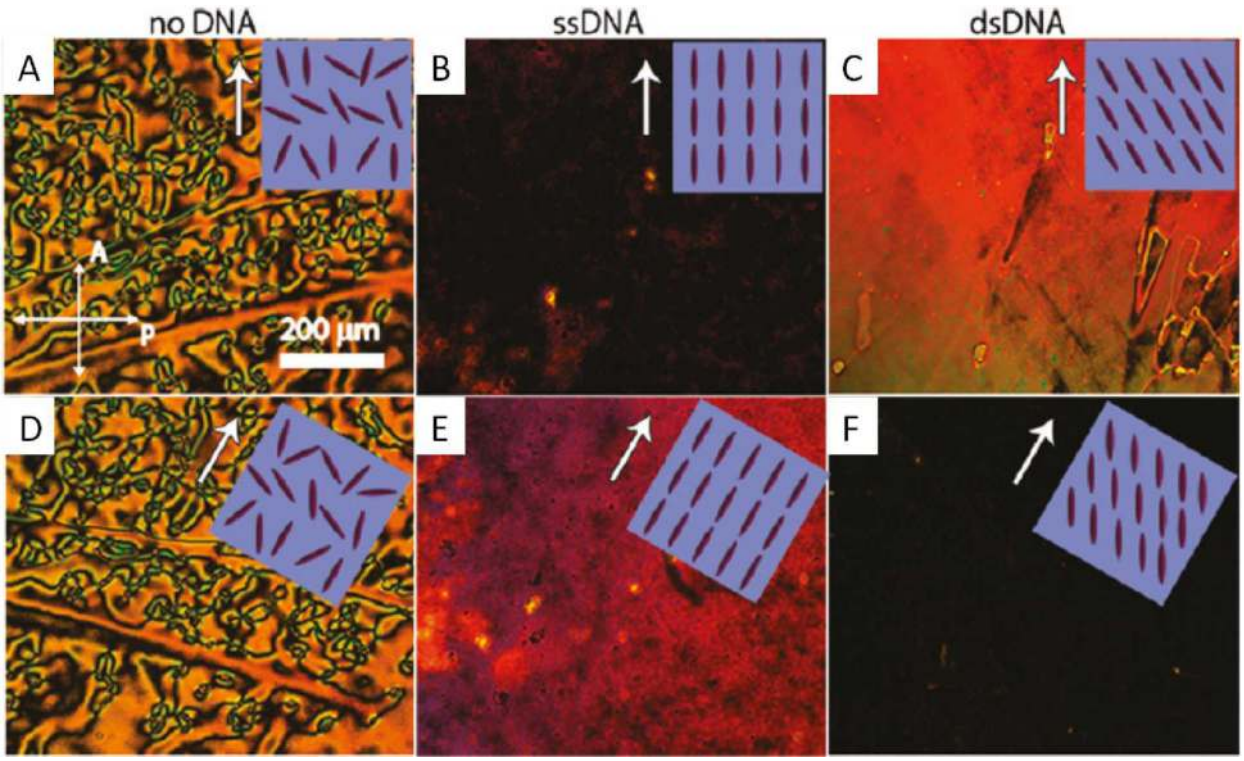

Figure 8.

Polarised light micrographs of LC (representative of either 5CB or MBBA, which had roughly the same surface orientation) on DNA-decorated surfaces. Crossed white arrows (in A) indicated the directions of the analyzer and polariser. White arrows indicate the direction of DNA extension where surfaces in (A-C) are aligned with the analyzer (i.e. 0° rotation) and surfaces in (D-F) are rotated by 30°. A dark micrograph indicates LC alignment in the direction of the polariser or analyzer (not homeotropic ordering). The cartoons in the inset show the alignment of the LC consistent with the respective micrographs. (A, D) Control sample contacted with buffer that did not contain DNA at 0° and 30° rotation, respectively. (B, E) ssDNA-decorated surface at 0° and 30° rotation, respectively. (C, F) dsDNA-decorated surface at 0° and 30° rotation, respectively. Reproduced with permission [41].

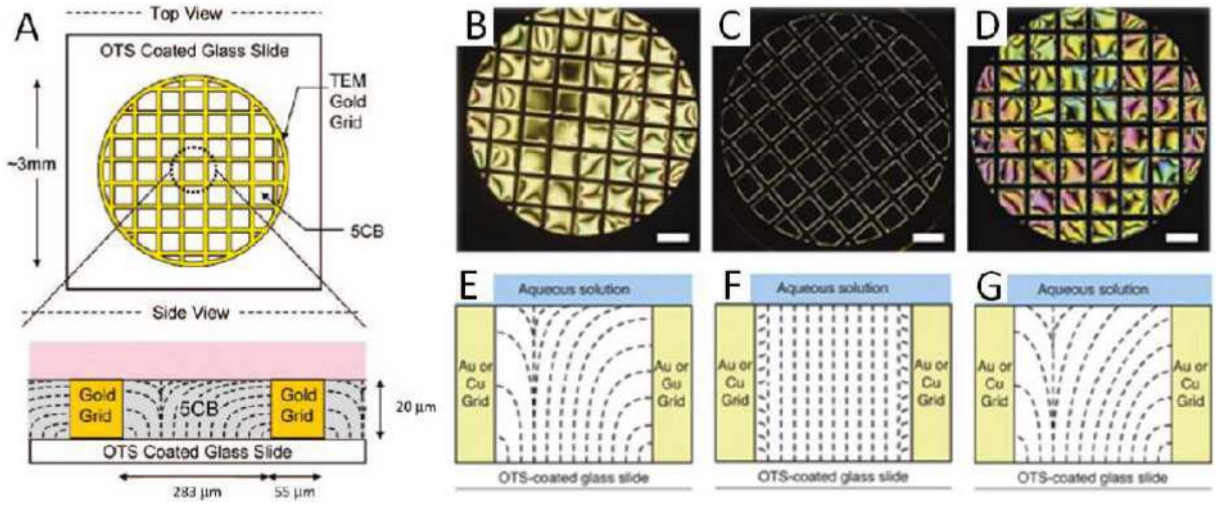

Figure 9.

Illustration of an LC film hosted in a TEM grid supported on an OTS-treated slide (A) and interpretations of the optical appearance of the LC-aqueous interface: planar (B, E); homeotropic (C, F); or tilted (D, G). Reproduced with permission [56].

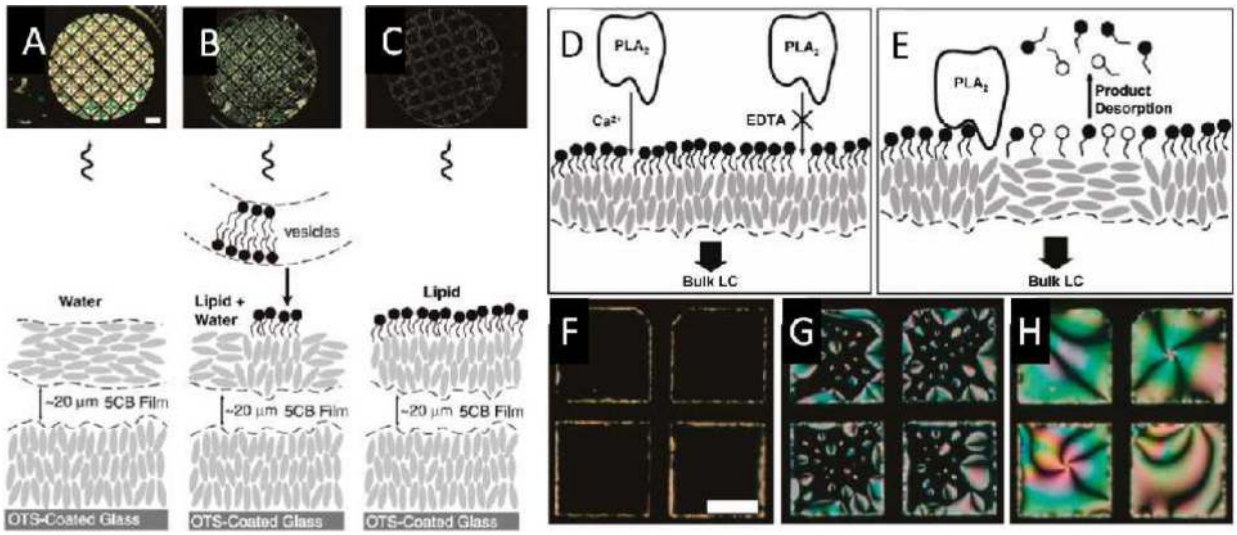

Figure 10.

Illustrations and optical micrographs (crossed polarisers) of (A-C) the formation of a phospholipid monolayer on an LC-aqueous interface and (D-H) enzymatic reaction occurring at the interface, leading to hydrolysis of the monolayer of phospholipid at the interface. Reproduced with permission [59, 61].

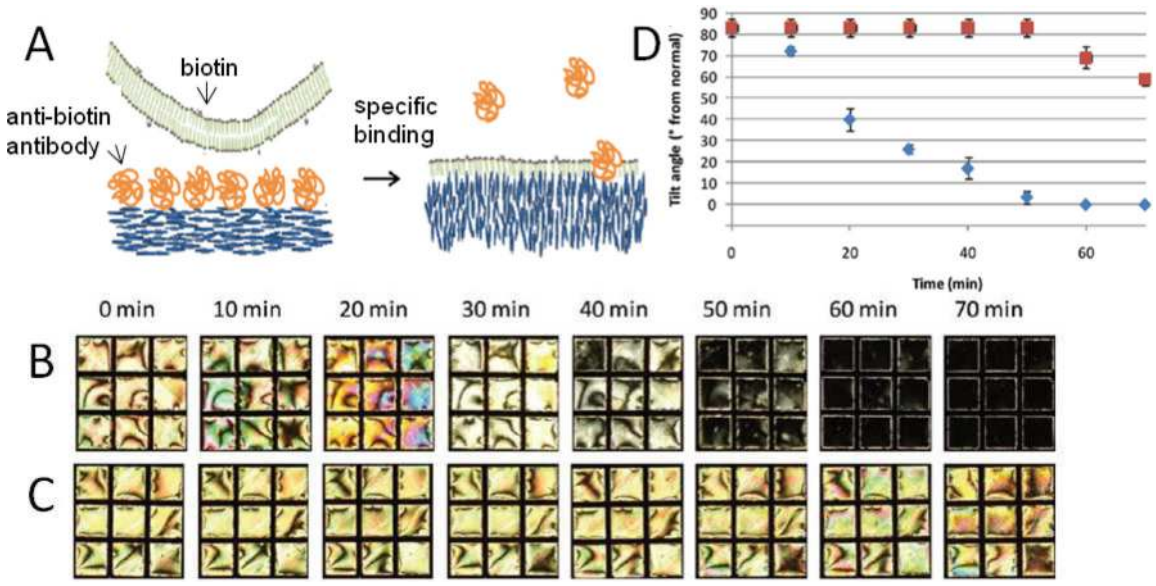

Figure 11.

Ordering transitions induced in films of 5CB by specific binding of biotinylated vesicles to anti-biotin antibody-decorated aqueous–5CB interfaces. (A) Schematic illustration of the specific capture of phospholipid on protein-decorated LC-aqueous interface. (B-C) Optical images (crossed polarisers) of 5CB that result from incubation of anti-biotin antibody-decorated interfaces against dispersions of vesicles containing (B) 5 mol % and (C) 0 mol % biotin-DOPE. (D) Tilt angle of 5CB at the LC-aqueous interfaces corresponding to (B) diamonds and (C) squares. Reproduced with permission [66].

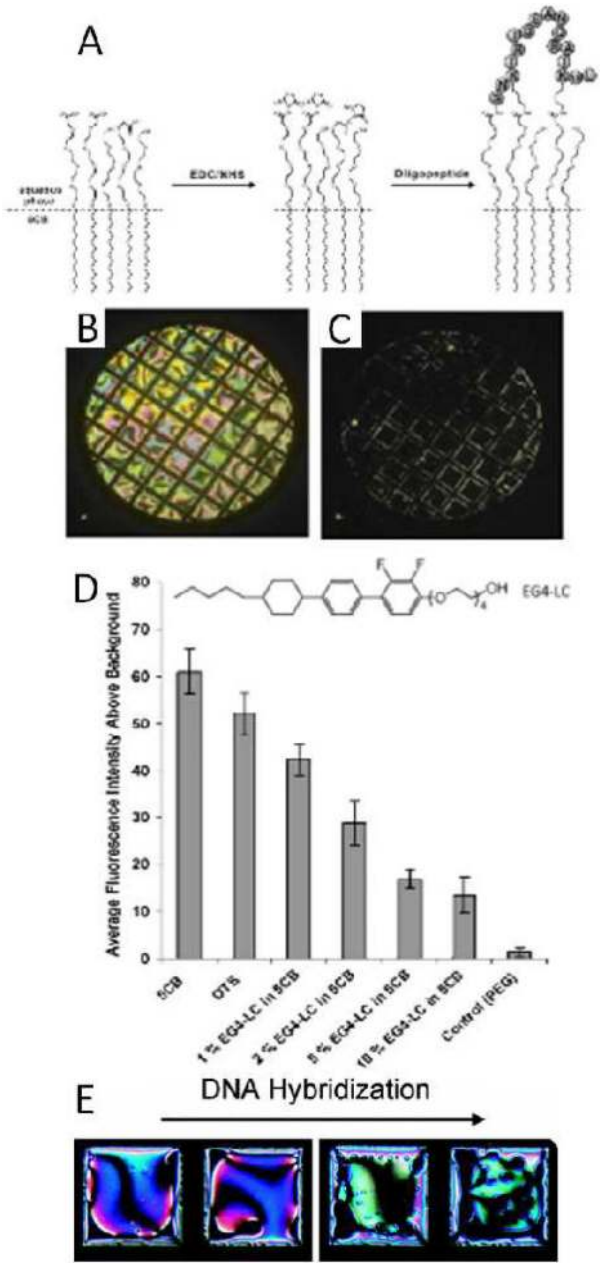

Figure 12.

(A) Schematic illustration of the formation of a surfactant-oligopeptide conjugate at the LC-aqueous interface; (B-C) Optical images of LC before (B) and after (C) enzymatic hydrolysis of the oligopeptide-surfactant conjugate at the interface (as shown in A). (D) Molecular structure of EG4-LC and measurements of non-specific adsorption of proteins to the interfaces of various materials, including 5CB doped with EG4-LC. (E) Ordering transition in an LC (E7) triggered by DNA hybridization at the surface of the LC (see text for details). Reproduced with permission [67, 71, 78].

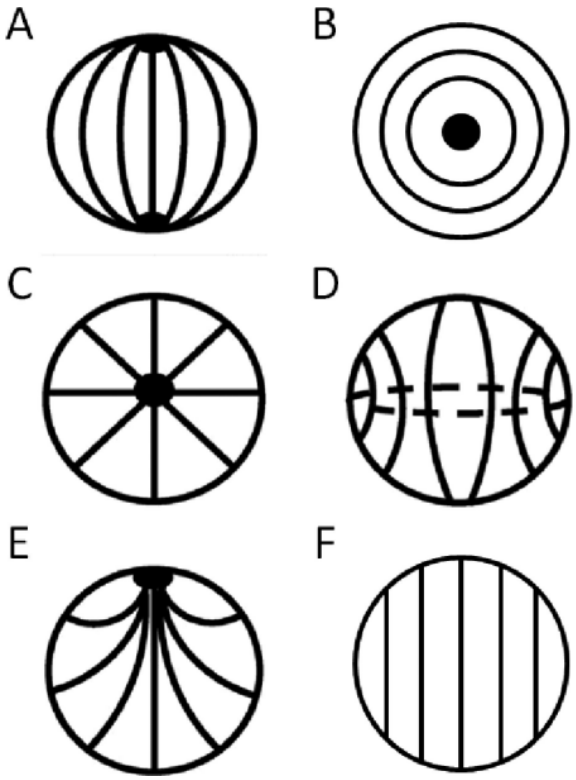

Figure 13.

Schematic illustrations of possible director configurations within nematic LC droplets under different anchoring conditions of the LC at the droplet surface. The solid black lines within the droplet boundaries represent the orientation of the director. Under planar (parallel) anchoring conditions the droplets can adopt (A) a bipolar configuration with two diametrically opposed surface point defects (boojums) at the poles of the droplet, or (B) a concentric (i.e. tordial or axial) configuration with a disclination line that traverses the diameter of the droplet, passing through the center of the sphere. Under normal anchoring conditions the droplets can adopt (C) a radial configuration possessing a central point defect at the core of the droplet, or (D) an axial (i.e. equatorial) configuration with a disclination line along the equator of the droplet. Under anchoring conditions between normal and planar the droplets can adopt (E) a pre-radial configuration. Another possible droplet configuration is (F) a uniform director profile.

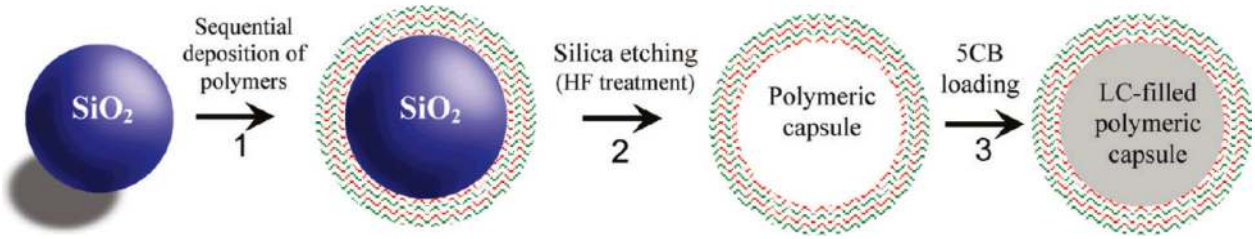

Figure 14.

Schematic illustration of the procedure used to prepare LC droplets of predetermined sizes within polymeric multilayer shells. Polymeric shells are prepared by sequential deposition of PSS and PAH onto silica templates and subsequent etching of the silica. The resulting polymeric shells are filled with LC (see text for details). Reproduced with permission [79].

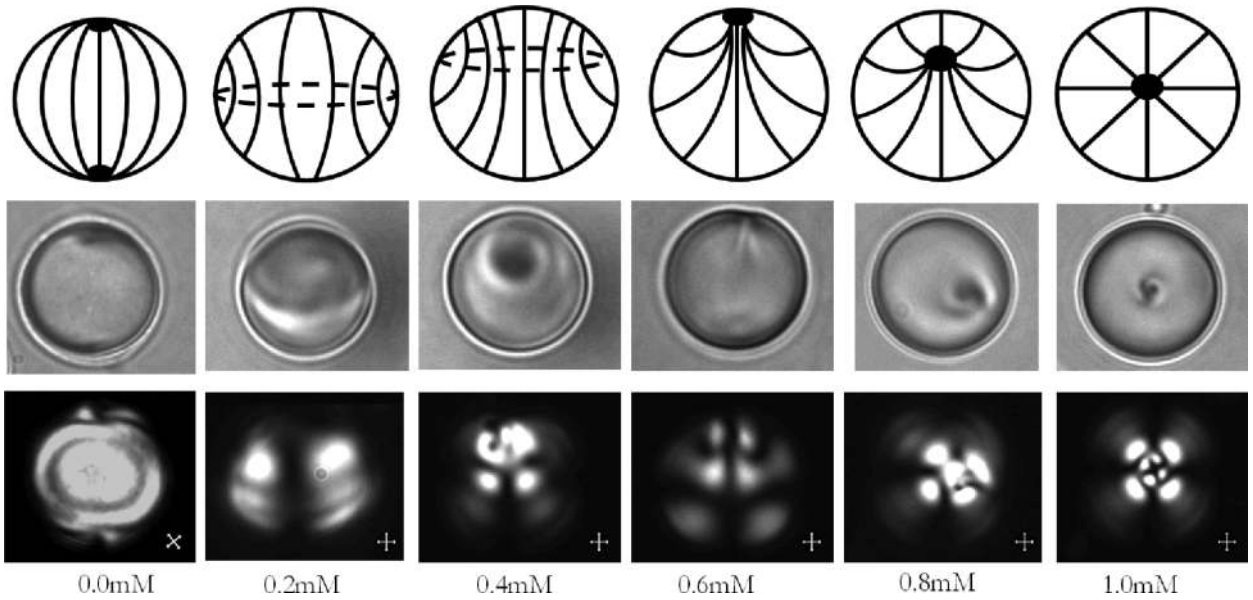

Figure 15.

Ordering transitions within LC droplets of fixed size induced by an adsorbate-driven change in the anchoring energy of the droplets. The change in surface anchoring of the LC droplet (from tangential to perpendicular) was achieved by equilibrating 8.0 ± 0.2-μm-diameter, polymer-encapsulated 5CB droplets with aqueous solutions containing SDS at concentrations that ranged from 0 to 1 mM (as indicated). The top row shows schematic illustrations of the configuration of the LC within each droplet, and the middle and bottom rows, respectively, show the corresponding bright-field and polarised light micrographs of the 5CB droplets. Reproduced with permission [79].

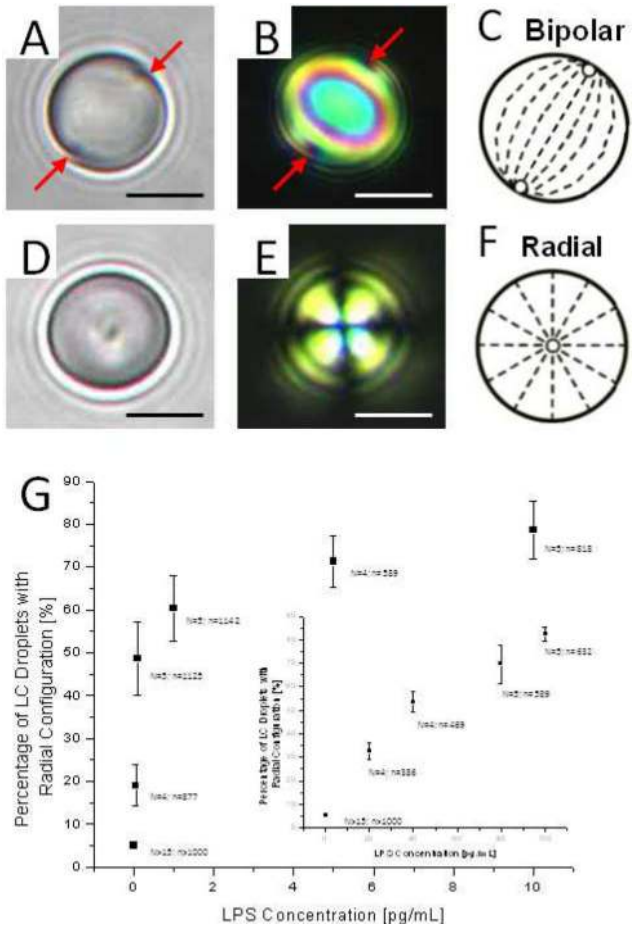

Figure 16.

Endotoxin-triggered bipolar-to-radial configurational transitions within water-dispersed μm-sized droplets of nematic 5CB. Bright-field (A) and polarised light (B, crossed polarisers) micrographs of a 5CB droplet in endotoxin-free water. The red arrows indicate boojums at the aqueous-LC interface of the droplet. (C) Schematic illustration of the bipolar configuration of the LC droplet corresponding to (A) and (B). Bright-field (D) and polarised light (E, crossed polarisers) micrographs of a 5CB droplet after exposure to endotoxin from *E. coli* (O127:B8; 1 mg/mL) in water. (F) Schematic illustration of the radial configuration of the LC droplet corresponding to (D) and (E). (G) Dose-response behaviour of the 5CB emulsion to different bulk concentrations of endotoxin. The outer graph displays the percentage of 8,300 LC droplets in 40 μL of water that exhibited a radial configuration, plotted as a function of endotoxin concentration, and the inset shows the response of the LC droplets when 94,000 droplets were used. Scale bars, 5 μm. Reproduced with permission [84].

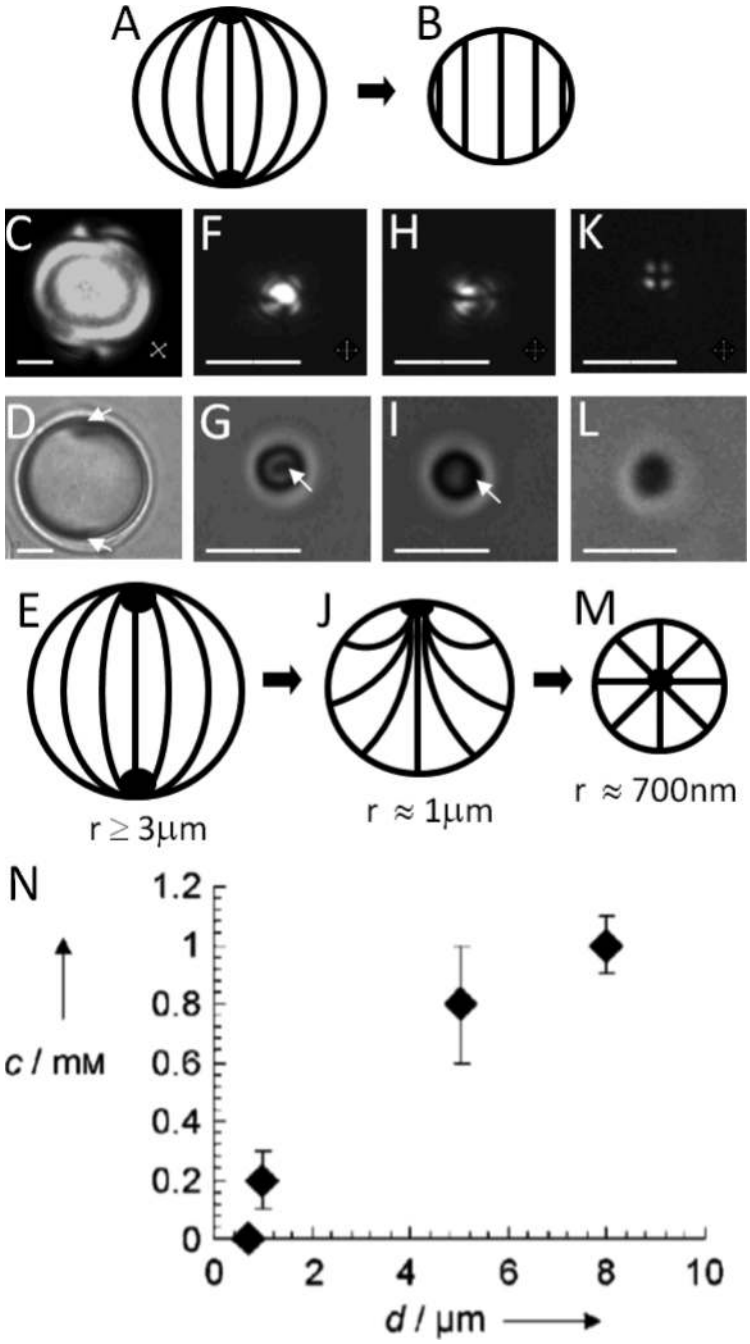

Figure 17.

Size-dependent ordering within LC droplets. (A) Bipolar and (B) uniform director configurations. (C, F, H, K) Polarised light and (D, G, I, L) bright-field optical micrographs of polymer-encapsulated 5CB droplets with (C, D) diameters of 8.0 ± 0.2 μm and bipolar LC ordering, (F–I) diameters of 1.0 ± 0.2 μm and preradial LC ordering (F and G show the end on views of the preradial ordering whereas H and I show side views), and (K, L) diameters of 0.70 ± 0.08 μm and radial LC ordering. Point defects in the LCs are indicated by white arrows. Cartoons in (E, J, and M) show bipolar, preradial, and radial ordering of the LC droplets, respectively. The scale bars are 2 μm for (C, D, and F–I), and 1 μm for (K, L). (N) Size-dependent response of

polymer-encapsulated LC droplets to concentration of model analyte (SDS). The SDS concentration (*c*) that causes radial ordering of the LC droplet is plotted as a function of droplet size (*d*). Reproduced with permission [80].

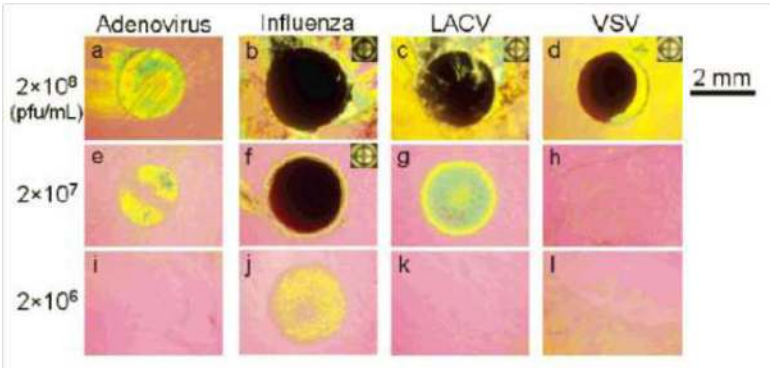

Figure 18.

Detection of lipid-encapsulated viruses using LCs. Poly-L-lysine treated gold slides were spotted with various virus-containing solutions to capture the virus on the surface. The virus bound on the surface was then contacted with nematic 5CB. The numbers on the left indicate the concentration of each virus suspension. Conoscopic images of the samples are provided in the insets in (b-d, f). All images were obtained immediately after the assembly of the liquid crystal cell. Reproduced with permission [104].

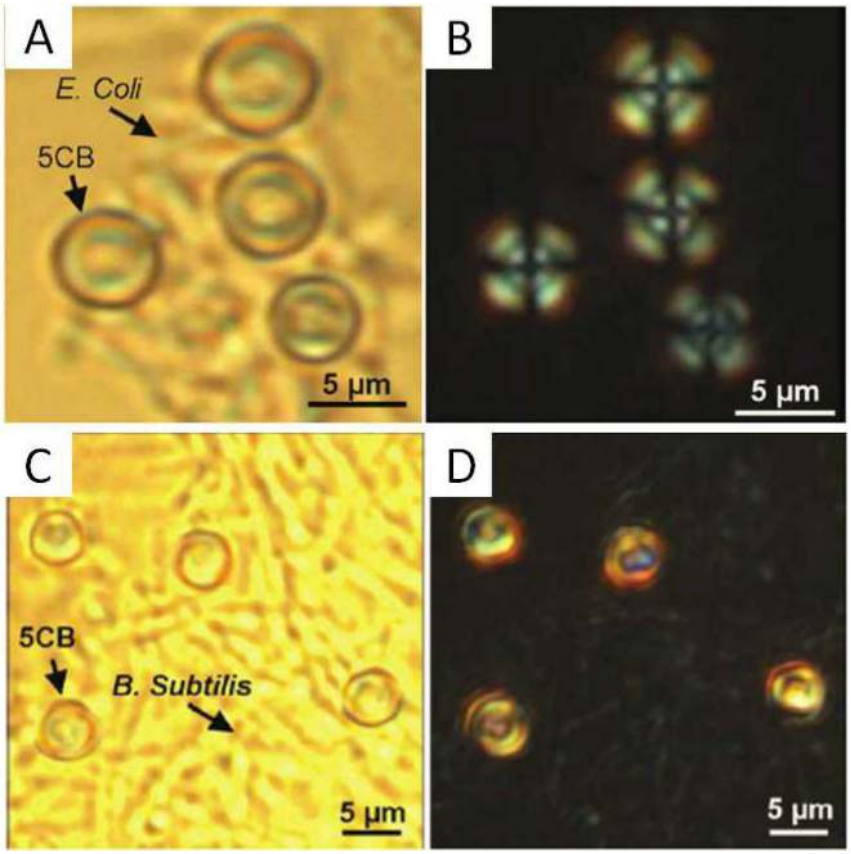

Figure 19.

Influence of gram-negative and gram-positive bacteria on the ordering within monodisperse micrometer-sized droplets of 5CB. (A) Bright-field and (B) corresponding polarised light (crossed polarisers) micrographs of 5CB droplets dispersed in an aqueous solution containing the gram-negative bacterium *E. coli* at a concentration of 5×10^5 cells/mL. The presence of *E. coli* caused a bipolar-to-radial ordering transition. (C) Bright-field and (D) corresponding polarised light (crossed polarisers) micrographs of 5CB droplets dispersed in an aqueous solution containing the gram-positive bacterium *B. subtilis* at a concentration of 6×10^5 cells/mL. The droplets remained in a bipolar configuration. Reproduced with permission [86].

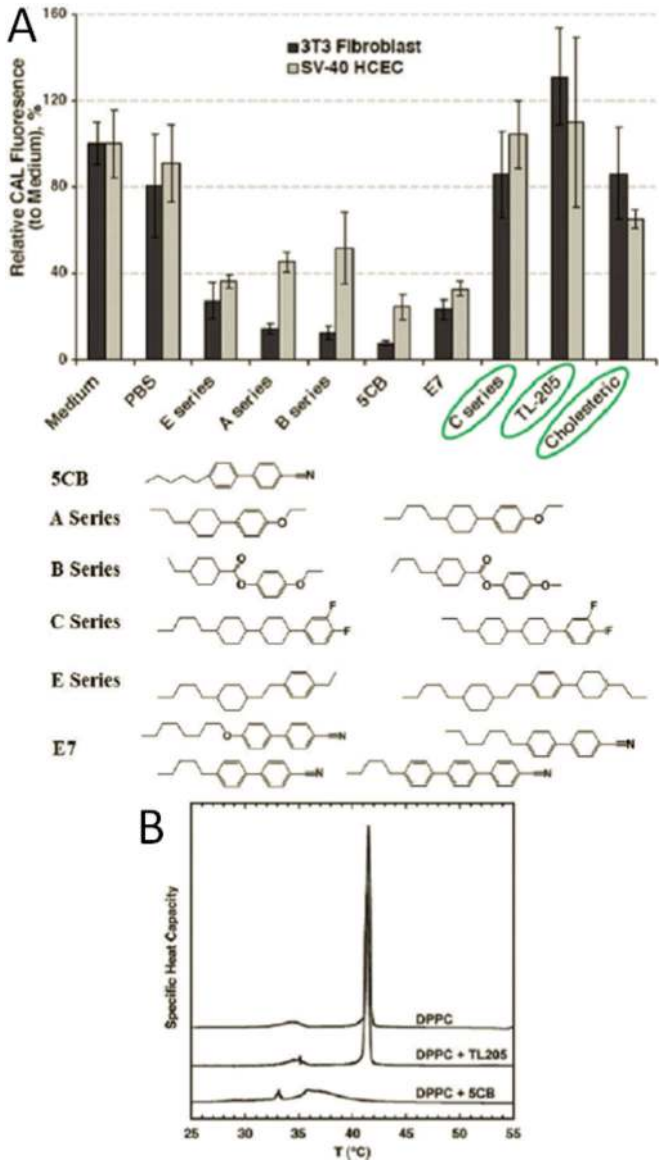

Figure 20.

(A) Relative intensities of fluorescence from CAL-AM added to 3T3 fibroblasts (black bars) and SV-40 HCECs (gray bars) following 4 h of contact of the cells with each LC indicated below the plot. The CAL fluorescence indicates the presence of living cells. (B) Endotherms (from differential scanning calorimetry) of DPPC multi-lamellar vesicle suspensions following seven days of incubation at 37 °C in the absence or presence of either TL205 or 5CB (as indicated). Reproduced with permission [107, 108].

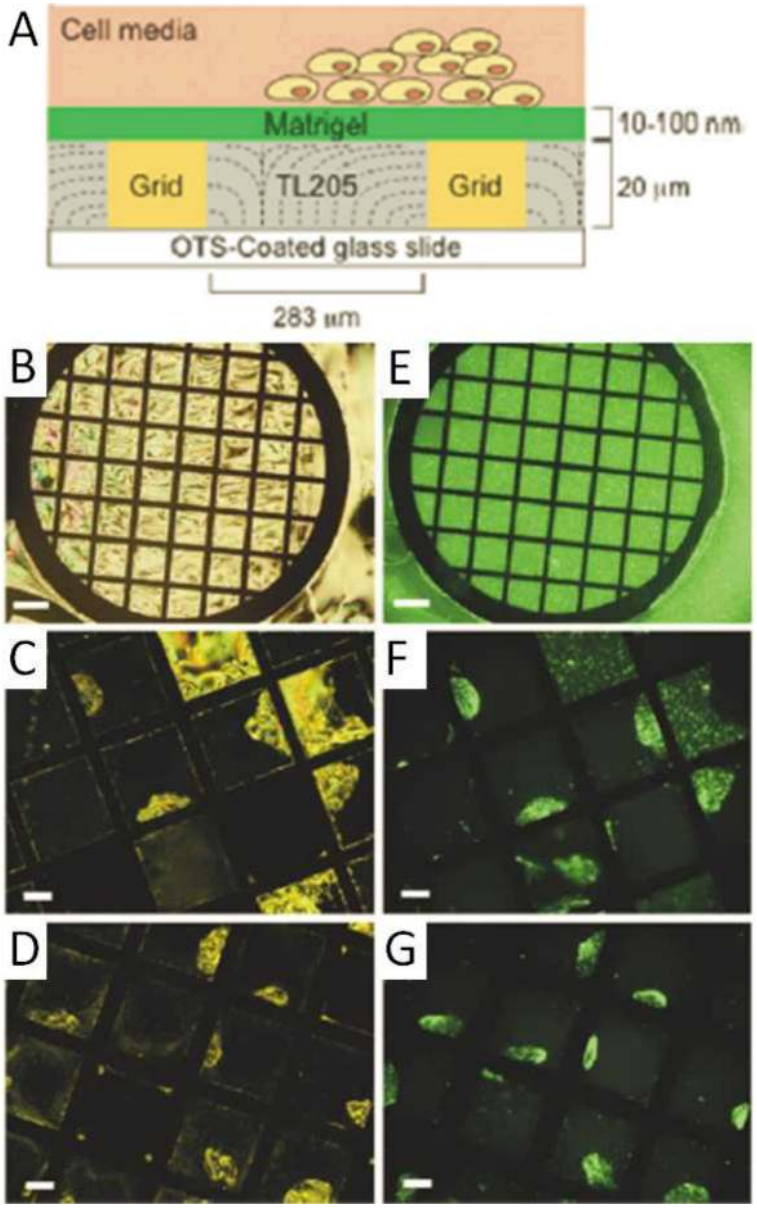

Figure 21.

(A) Schematic illustration of human embryonic stem cells (hESCs) cultured at the interface between aqueous phases and nematic TL205. (B-D) Polarised light and (E-G) epifluorescence images of hESCs before the seeding of cells (B, E), 3 days following seeding (C, F) and 7 days following seeding (D, G). The Matrigel was labelled with Alexa Fluor 430. Scale bars are 300 μm for (B, E); all others are 100 μm. Reproduced with permission [111].

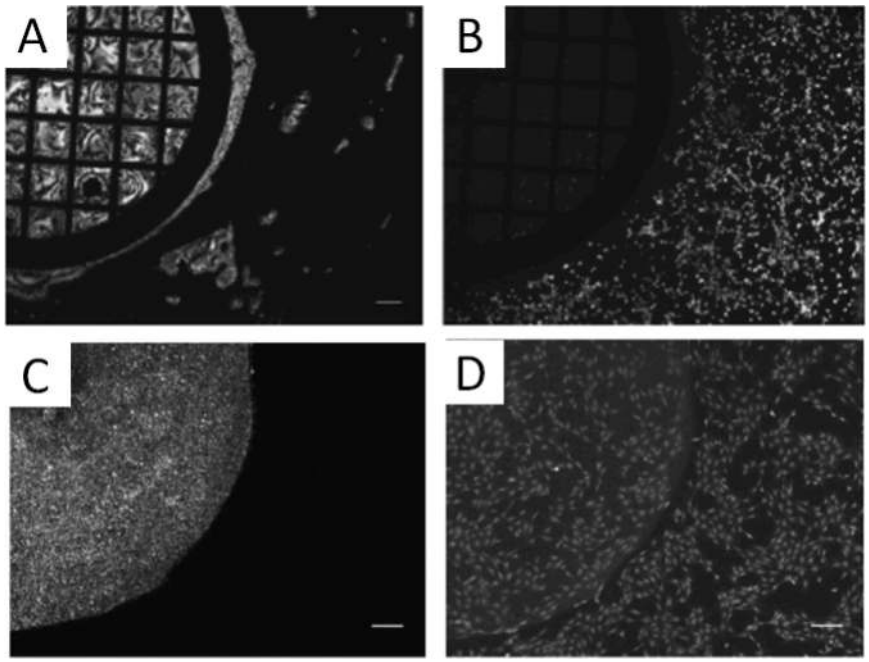

Figure 22.

Fibroblast cells seeded on both a TEM grid containing nematic phase E7 (A, B) and a colloid-in-LC gel formed with E7 (C, D) were stained with Calcein AM and imaged using polarised light (A, C) and epifluorescence (B, D). Cells were only able to grow on the CLC gel. Scale bar is 200 μm in (A) and 100 μm in (C, D). Reproduced with permission [112].